UNIVERSITY OF CALIFORNIA
RIVERSIDE

Identification of Chemicals with the Potential to Help Maintain Pluripotency of Human Embryonic Stem Cells in a Suspension Bioreactor

A Thesis submitted in partial satisfaction
of the requirements for the degree of

Master of Science

in

Bioengineering

by

Christina Oviya Jones Tarcius Doss

December 2024

Thesis Committee:

Dr. Nicole zur Nieden, Chairperson
Dr. Joshua Morgan
Dr. Sarah H Radi

The Thesis of Christina Oviya Jones Tarcius Doss is approved:

_____

_____

_____

Committee Chairperson

University of California, Riverside

ACKNOWLEGEMENTS

I first thank God for granting me the strength, wisdom, grace, and mercy to complete this project.

I am deeply grateful to Dr. Nicole zur Nieden for providing me with the opportunity where I was able to accomplish because of her patience and guidance throughout my work. I also want to express my thanks to Dr. Thomas Später for his constant support and insights. A special thanks to all my lab mates, especially Dr. Ariana Hardy and Ruthia Soh, for teaching me and helping me with the experiments.

I would like to extend gratitude to the Department of Bioengineering and all my professors for offering me the opportunity to grow professionally.

I am also sincerely grateful to my committee members Dr. Joshua Morgan and Dr. Sarah H Radi for their unwavering support, understanding, and guidance.

I am truly thankful to my friends and family for all the encouragement and love they have shown me. A special thank you to my parents for always being there when I needed them the most, and to my sisters, who I love dearly.

ABSTRACT OF THE THESIS

Identification of Chemicals with the Potential to Help Maintain Pluripotency of Human Embryonic Stem Cells in a Suspension Bioreactor

by

Christina Oviya Jones Tarcius Doss

Master of Science, Graduate Program in Bioengineering
University of California, Riverside, December 2024
Dr. Nicole zur Nieden, Chairperson

The unique combination of their self-renewal and potency has heightened demand for pluripotent stem cells (PSCs), including embryonic stem cells (ESCs) and induced pluripotent stem cells, making their mass production a major focus in regenerative medicine and tissue engineering research. Allowing for large-scale stem cell production, suspension bioreactors are emerging as a promising alternative to traditional tissue culture dishes. Bioreactors offer a controlled environment that facilitates the mass growth of PSCs by regulating specific conditions, including oxygen levels, nutrient composition, and shear stress. However, human PSCs are sensitive to fluctuations in these conditions, which can result in unwanted differentiation. Indeed, our previously conducted global transcriptome analyses revealed two populations of cells upon bioreactor culture, one with a naïve pluripotent transcript signature and another more differentiated one. This sensitivity to unwanted differentiation necessitates precise control over factors such as growth media and culture additives.

Therefore, the present study explores the complex and poorly understood signaling pathways that regulate cell fate in suspension bioreactors aiming to identify compounds that sustain

pluripotency in a bioreactor environment. Twenty-one differentially expressed candidate kinases and receptors were identified from the previous RNA sequencing data set. Next, a plate-based chemical screening assay was conducted to evaluate both activators and inhibitors of identified candidate pathways. To determine the effects of these chemicals on stem cell pluripotency, colonies were stained for alkaline phosphatase and imaged. Several quantification methods utilizing ImageJ FIJI software were implemented to analyze the morphology, proliferation, and quality of colonies. Among these methods, a novel characterization approach was proposed, and method optimization enhanced reliability and accuracy, improving stain quantification and morphological analysis. For example, this image-based quantification of pluripotency revealed that the chemicals utilized for the activation of PI3K (740 Y-P TFA), MAPK (Asiatic acid), and inhibition of TGFβ (LY2157299) and FAK (Y15) pathways significantly enhanced cellular pluripotency. Altogether, this study serves as a preliminary screening method that revealed potential molecular targets and mechanisms that govern self-renewal, leading to the identification of chemical combinations with the potential to sustain pluripotency in human embryonic stem cells within bioreactor systems.

TABLE OF CONTENTS

LIST OF FIGURES

LIST OF TABLES

1 INTRODUCTION

1.1 Stem Cells

Each organ in the body contains stem cells that play a crucial role in the maintenance and repair of tissues. Stem cells are unique cells in the body that have the remarkable potential to develop into many different cell types. They serve as a repair system, capable of dividing without limit to replenish other cells as long as the person or animal is alive. Stem cells are pivotal for advancing medicine and research due to their potential to reveal developmental processes and the origins of various conditions. In regenerative medicine, stem cell-based therapies show immense promise for treating diseases by restoring physiological function through cell replacement or stimulating the body's natural repair mechanisms. These approaches have the potential to revolutionize treatments for a wide range of conditions, offering hope for improved outcomes and personalized therapies. (Xu et al., 2008; Amabile & Meissner., 2009; Apati et al., 2018). The main types of stem cells are Embryonic Stem Cells (ESCs) are Pluripotent Stem Cells (PSCs), meaning they can differentiate into nearly any cell type in the body that are used in regenerative medicine for studying early human development and drug testing.

ASCs are multipotent or unipotent, meaning they have a limited ability to differentiate into specific cell types. They reside in specialized niches that regulate their activity. ASCs have been identified in tissues like the hematopoietic system (HSCs), central nervous system, liver, skin, cornea, gut, skeletal muscle, adipose tissue, and bone marrow (e.g., mesenchymal stem cells or MSCs) (Yang et al., 2017; Lange et al., 2022). ASCs play vital roles in regenerative medicine due to their differentiation potential and bioactive molecule secretion, showing promise in treating injuries, inflammation, and age- degeneration. Further research is needed to enhance their

therapeutic potential and address challenges like cell heterogeneity (NRC 20002; Ahsan et al., 2008; Komal Loya,2014; Audronė et al.,2017).

Induced pluripotent stem cells (iPSCs) are reprogrammed adult cells (e.g., skin or blood) reverted to a pluripotent state using key transcription factors (OCT4, SOX2, KLF4, and c-MYC) (Waring et al., 2015; Cerneckis et al., 2024). Discovered by Takahashi and Yamanaka in 2006, this groundbreaking method bypasses the ethical concerns of embryonic stem cells, earning him a Nobel Prize. iPSCs, like embryonic stem cells, can differentiate into nearly any cell type and self-renew indefinitely, making them invaluable for regenerative medicine, personalized therapies, drug testing, and disease modeling while reducing the risk of immune rejection (Takahashi et al., 2007; Huangfu et al., 2008; Ben-David et al., 2013). Despite their promise, iPSCs face challenges, including genetic/epigenetic instability and risks of tumor formation due to the reprogramming process. Maintaining iPSCs in culture requires carefully controlled conditions to prevent loss of pluripotency and unwanted differentiation. Issues such as cell aggregation and heterogeneity complicate the production of pure, uniform populations, limiting their therapeutic potential (Jaenisch, 2004; Kim et al., 2022). Addressing these challenges is crucial to advancing iPSC-based clinical applications (Lyssiotis et al., 2009; McLaren et al., 2013; Romito & Cobellis, 2016; Li et al., 2018).

Understanding the mechanism behind self-renewal could reveal how cell fate is regulated during embryonic development, post-natal growth, aging, and cancer. Such information may also enable scientists to grow stem cells in the laboratory.

1.1.1 Totipotent Stem Cells

The earliest totipotent stem cells are zygote formed after fertilization which has unique ability to differentiate into an entire organism, including all embryonic and extra-embryonic

tissues. The zygote undergoes sequential cleavage into smaller cells called blastomeres, progressing from a single cell to two, four, and eventually eight cells in 1 to 3 days. During these early divisions, each blastomere remains totipotent, retaining the potential to develop into a complete organism if isolated. By the time the embryo reaches the 16-32 cell stage in 3 to 4 days, it resembles a morula. At this stage, the cells begin to compact and interact more closely with one another. Totipotency gradually diminishes as cells continue dividing and differentiating. Some cells start to commit to specific roles in embryonic or extra-embryonic tissues. The morula transforms into a blastocyst in 5 to 6 days. The blastocyst comprises two distinct layers, which are the outer cell mass (trophoblast or trophectoderm) and the inner cell mass (ICM or embryoblast). The trophectoderm contributes to the formation of extra-embryonic tissues, which later develop into structures like the placenta, chorion, and umbilical cord. The embryoblast develops into the embryo itself. The cells in the ICM are no longer totipotent but are now pluripotent, meaning they can form most but not all cell types (placental tissues). Once the blastocyst forms, totipotency is lost (Gilbert, 2006; Lu & Zhang, 2015; Tabansky & Stern 2016; Genet &Torres-Padilla, 2020).

1.1.2 Pluripotent Stem Cells

Pluripotent stem cells have the potential to differentiate into all the three germ layers among in vitro-derived stem cells, capable of generating all adult cell types (Keller, 2005; Sirenko et al., 2013; Romito & Cobellis, 2016). The germ layers are the three primary layers of cells formed during early embryonic development, which give rise to all the tissues and organs of the body. These germ layers are fundamental in establishing the body's basic structural and functional organization during development. These germ layers are ectoderm that gives rise to the skin, nervous system (including the brain and spinal cord), and other tissues like hair and nails, mesoderm that forms structures such as muscles, bones, the circulatory system, kidneys, and reproductive organs and

endoderm that develops into internal organs such as the lungs, liver, pancreas, and digestive system (Evans & Kaufman, 1981; Martin, 1981; Thomson et al., 1998). Naïve pluripotency is the earliest and most primitive state of pluripotent stem cells, resembling pre-implantation epiblast cells. These cells are highly pluripotent and express core pluripotency genes (Oct4, Sox2, NANOG). In contrast, primed pluripotency represents a more advanced state, poised for differentiation and resembling post-implantation epiblast cells. Different phases of pluripotency, like naive and primed, have been identified and stabilized with specific culture conditions (Brons et al., 2007; Nichols & Smith, 2009).

1.2 Ways To Maintain Pluripotency

Pluripotent stem cells are typically cultured in static vessels, either as adherent monolayers or as non-adherent spherical aggregates. While this method is adequate for generating cells for experimental use, it is impractical for producing the large quantities needed for clinical or commercial applications. For PSC-based therapies, the required cell dosages can range from 10^9 to 10^{12} cells per patient, depending on the specific therapeutic target. To meet these demands effectively, scalable bioreactors must be utilized. Such bioreactors offer several advantages, including lower operating and labor costs, enhanced scalability, and improved process control capabilities. Previous research indicates that expanding hPSCs as aggregates in stirred suspension bioreactors provides notable production advantages over traditional static cell culture methods. These bioreactor systems enable the control and standardization of key physiological parameters, leading to the generation of high-quality batches with substantial cell yields (Krawetz et al., 2010; Rodrigues et al., 2011; Rohani et al., 2020).

A pluripotent stem cell suspension bioreactor is designed to culture PSCs in a liquid environment, maintaining their pluripotency and viability for scalable applications in research,

regenerative medicine, and tissue engineering. The type of bioreactor and its design significantly impact the growth, expansion, and differentiation potential of PSCs. Some common bioreactor types are Stirred-Tank bioreactors, used for large-scale PSC culture with mechanical stirring, Wave -bioreactors which use gentle rocking and are ideal for smaller-scale applications, and Air-Lift bioreactors which injects air for gentle mixing and efficient gas exchange. In Suspension bioreactors the cells are kept in suspension through agitation (mechanical stirring, air sparging, or rocking), ensuring even distribution of nutrients, gases, and growth factors. Oxygen is provided via air or oxygen-enriched gas to meet the cells' high metabolic demands. The bioreactor controls temperature, pH, and nutrients, and uses waste removal systems to improve cell health. In addition to bioreactor, media are crucial components in the culture and expansion of PSCs. Bioreactors provide the necessary environment to culture PSCs at large scale, while media supply the nutrients, growth factors, and conditions needed to maintain the pluripotent state and support cell health. Together, they enable the production of high-quality PSCs for research, clinical applications, and regenerative medicine. In bioreactors, media are continuously replenished, with tightly controlled factors like oxygen, pH, and nutrients to sustain pluripotency, minimizing immune rejection risks in therapeutic applications (Kehoe et al., 2010; Wang et al., 2013).

Bioreactors offer scalable stem cell expansion but have limitations that can alter cell fate. Challenges include shear stress, uneven nutrient distribution, unintended differentiation, cell aggregation, loss of stemness, and variability during scale-up. These issues may lead to cell damage, differentiation, or senescence. Addressing them requires optimizing bioreactor design, monitoring systems, and leveraging pathways like Wnt signaling to maintain stemness and control cell behavior.

Research has shown that the culture environment—including feeder cells, extracellular matrices, and signaling molecules such as Wnt, FGF, and BMP—strongly influences alkaline phosphatase (ALP) activity. Notably, Wnt signaling plays a key role in sustaining pluripotency, with its modulation significantly impacting ALP activity (Blauwkamp et al., 2012).

1.2.1 Media composition

Media are liquid solutions that provide essential nutrients, vitamins, growth factors, and hormones to support the growth and maintenance of PSCs while preserving their undifferentiated and pluripotent state. Cell culture media typically include amino acids, carbohydrates, salts, vitamins, and buffering agents, with optional supplements like serum and growth factors. Specialized media, such as mTeSR, are designed for long-term PSC culture without feeder cells or serum, ensuring consistency and reliability for research and clinical applications (Ludwig et al., 2006; Lanon et al., 2008). Essential 8 (E8) is a simplified serum-free and xeno-free medium containing eight essential components, including bFGF, TGF-β, insulin, and ascorbic acid, designed for efficient and high-quality maintenance of hPSCs without animal-derived components, making it suitable for clinical applications. Knock Out DMEM and StemPro™ are also widely used for supporting hESCs and iPSCs, with supplements like bFGF to enhance growth and maintain pluripotency. Proper media selection is vital for optimal cell growth and therapeutic potential. mTeSR1 and E8 are the most commonly used media for hPSC culture.

1.2.2 Growth Factors

Growth factors are essential for culturing PSCs, working synergistically with culture media to maintain their undifferentiated state, promote self-renewal, and ensure growth and viability. Key growth factors include bFGF, critical for preventing differentiation and promoting PSC

proliferation, included in media like mTeSR1 and E8, Activin A which maintains pluripotency by activating the SMAD signaling pathway, TGF-β which regulates pluripotency and prevents differentiation into endodermal and mesodermal lineages ,LIF essential for sustaining pluripotency in mouse embryonic stem cells (mESCs) and additional factors like insulin, transferrin, selenium, ethanolamine, sodium pyruvate, and ascorbic acid that support hPSC survival and self-renewal, further enhancing culture efficiency.

Growth factors and small molecule inhibitors maintain pluripotency by blocking differentiation pathways. Fibroblast Growth Factor 2 (FGF2) is a potent activator of MAPK/ERK signaling and can also stimulate PI3K. In the culture medium of hESCs, the presence of basic fibroblast growth factor (bFGF) activates the epidermal growth factor receptor (EGFR) and the insulin-like growth factor 1 receptor (IGF1R), which in turn stimulates both the PI3K and MEK/ERK signaling pathways (Turner &Grose, 2010).

1.2.3 Small Molecule Inhibitors

Small molecule inhibitors are sometimes added to the culture media to block signaling pathways that would otherwise lead to differentiation.

GSK-3 Inhibitors (CHIR99021) are often used to activate the Wnt signaling pathway, which is involved in maintaining pluripotency and promoting cell proliferation. MEK Inhibitors (PD0325901) are used to inhibit the MAPK/ERK signaling pathway, which helps maintain stem cell self-renewal. Activin A and TGF-β help prevent cells from differentiating into endodermal or mesodermal lineages, keeping them in an undifferentiated state. In the case of iPSCs, specific growth factors and small molecules are used to reprogram somatic cells back into a pluripotent state (Huang et al.,2017).

Maintaining the pluripotency of hESC relies on the interplay of various signaling pathways. The interaction between these pathways adds complexity, as there is dependent crosstalk between them, occurring both directly and indirectly. The design of a reproducible and robust bioprocess should be dynamic, incorporating ongoing efforts to understand how the process will respond over time and under various stresses. This understanding is essential before moving into large-scale production, where these stresses will be intensified.

1.3 Signaling Pathways

Signaling pathways are central to maintaining pluripotency and regulating the behavior of stem cells. They respond to external signals and direct the internal machinery of cells, ensuring that stem cells self-renew when necessary and differentiate into specialized cell types under the right conditions. Understanding and manipulating these pathways is essential for advancing stem cell research, regenerative medicine, and therapies for various diseases. These pathways are tightly regulated, and disruptions in these signaling networks can lead to loss of pluripotency, uncontrolled differentiation, or tumor formation. Key pathways include TGF-β/SMAD for maintaining pluripotency in hPSCs that activate SMAD proteins to regulate gene expression. Inhibition of this pathway promotes mesoderm and endoderm differentiation. FGF/ERK pathway is essential for self-renewal and proliferation. bFGF activates the ERK/MAPK pathway to support the undifferentiated state. Wnt/β-Catenin pathway regulates pluripotency or differentiation based on β-catenin stabilization. LIF/STAT3 pathway promotes self-renewal in mouse ESCs but is not effective in human PSCs. PI3K/AKT pathway supports cell survival, metabolism, and self-renewal by activating AKT signaling. Notch signalling pathway influences cell fate decisions and self-renewal by regulating gene expression through Notch intracellular domain (NICD). A variety of synergistically working signaling pathways, including the Wnt signaling, p38 MAPK, PI3K, insulin

growth factor (IGF)/insulin, CK1a, SHP2, IRS1, LKB1, PGDFR, JNK, EGFR, PKC, TGF, and PAK, FAK, TAK pathways, regulate the fate of hPSCs in culture while relying on growth factor supplementation.

1.4 Pluripotency Assays

Assaying pluripotency ensures the quality, functionality, and safety of pluripotent stem cells (PSCs) such as ESCs and iPSCs. It verifies their ability to self-renew, differentiate into all three germ layers, and maintain genomic stability. This is essential for authenticating cell identity, guaranteeing functional potential, maintaining culture consistency, meeting safety standards for clinical use, and supporting reliable research. Pluripotency assays are vital for advancing both basic science and therapeutic applications, reducing risks in regenerative medicine and ensuring high-quality outcomes.

The alkaline phosphatase (ALP) assay is commonly used to assess pluripotency in stem cells, particularly ESCs and iPSCs. ALP enzyme expression and activity are primarily regulated by the developmental status of cells and tissues. This regulation makes ALP a valuable marker for tracking differentiation processes in both in vivo and in vitro settings. High ALP activity is characteristic of pluripotent stem cells, such as embryonic stem and induced pluripotent stem cells, reflecting their undifferentiated state. As differentiation proceeds, ALP activity decreases, marking the transition from a pluripotent state to lineage commitment (Stefkova et al., 2015). This regulation of ALP underscores its utility in monitoring differentiation and lineage specification (Caverzasio & Manen, 2007). This characteristic is based on the high ALP activity observed in the inner cell mass (ICM) of the blastocyst stage, in contrast to trophoblast cells, which do not exhibit high ALP levels. As the ICM differentiates into specialized lineages, ALP expression diminishes, but it remains present in specific cell populations like primordial germ (PG) cells and reappears in

certain tissues, such as osteoblasts, during development. Most pluripotent stem cells, including embryonal carcinoma (EC) cells, embryonic germ (EG) cells, embryonic stem cells, and induced pluripotent stem cells, exhibit high ALP activity, marking their undifferentiated state and pluripotency. Epiblast stem cells, derived from the epiblast of later embryonic stages, show an absence of ALP activity. These cells possess more restricted pluripotency compared to ESC, reflecting their more differentiated phenotype (Brons et al., 2007; Tesar et al., 2007).

In experiments, ALP staining is used to visualize pluripotent colonies, often resulting in distinct color changes (e.g., pink, purple, or blue) upon staining. Positive ALP staining suggests pluripotency, while reduced or absent staining implies differentiation (Martello & Smith 2014). ALP staining was one of the initial assays used to validate successful reprogramming when iPSCs were first generated from somatic cells (Takahashi Yamanaka, 2006), High ALP activity was a hallmark of reprogrammed cells, akin to ESCs, indicating that these cells had regained pluripotency. Researchers have effectively utilized ALP staining to monitor the differentiation processes of pluripotent stem cells. In various studies involving directed differentiation protocols, a notable reduction in ALP staining was observed, indicating that the cells were transitioning from a pluripotent state to specialized cell types. This correlation provides a useful marker for tracking differentiation. Additionally, comparative studies assessing ALP expression across different stem cell lines have revealed variations in ALP activity. ALP staining is a crucial quality control tool in stem cell research, particularly for large-scale culture and expansion. It provides a rapid, cost-effective method to confirm that stem cell cultures remain undifferentiated, ensuring reliability for experimental or therapeutic applications in regenerative medicine and disease modelling. ALP staining is widely used to monitor pluripotency throughout preclinical phases.

1.5 From Pixels to Precision: Navigating the World of Image Analysis

While visual assessment of ALP staining offers a qualitative overview, quantitative analysis is critical for accurate and reproducible evaluations. It enables objective comparisons of pluripotency across different cell populations, culture conditions, or treatments, making it an indispensable method in pluripotency and differentiation studies.

ImageJ is a powerful, open-source software widely used in biological research for image acquisition and analysis, including ALP staining in stem cell studies. Its cost-effectiveness and accessibility make it a valuable alternative to expensive commercial software, particularly for labs with limited resources. Developed with a focus on biological applications, ImageJ's extensible plugin architecture and custom macro capabilities enable tailored, automated, and batch processing of large datasets. These features reduce user bias, improve efficiency, and support a wide range of microscopy-based quantifications (Jensen, 2013).

For ALP staining, ImageJ allows colony-level analysis, providing both staining intensity and spatial context. This enables detailed examination of heterogeneity within stem cell cultures, which bulk methods cannot address. It also supports morphometric analyses, offering metrics such as stained colony counts, staining intensity, total stained area, and colony morphology. Researchers can visually inspect images alongside quantitative data, ensuring accuracy and reliability. ImageJ's ability to process multiple images simultaneously and its background subtraction and normalization features improve consistency and data quality.

Fiji, an enhanced version of ImageJ, bridges biology and computer science by enabling collaboration and integrating advanced algorithms for biological challenges. While ImageJ has many advantages, it requires standardized imaging conditions to avoid variability. Inconsistent lighting or staining can affect results, and manual analysis may introduce subjectivity if not

automated. Despite these limitations, ImageJ provides a versatile, precise, and non-destructive approach for ALP staining analysis, preserving samples for downstream studies and long-term storage.

The Tagged Image File Format (TIFF) is commonly used in scientific applications due to its uncompressed nature and ability to store embedded metadata, which is crucial for accurate interpretation and reproducibility of results. TIFF files contain essential information such as image scaling, laser wavelengths, and other parameters that ensure consistent image analysis.

Bit Depth refers to the number of bits used to represent the color or intensity of each pixel in an image. It determines the image's color range, quality, and dynamic range. 8-bit depth provides 256 shades per channel (16.7 million colors), common in digital images and web graphics. 16-bit depth offers 65,536 shades per channel (281 trillion colors), used for high-quality images, allowing smoother gradients and more detailed color information. 32-bit depth is used for High Dynamic Range (HDR) imaging, representing over 4 billion colors, with an additional alpha channel for transparency (Cheng et al 2001).

Higher bit depths capture a wider range of brightness levels, making them suitable for post-processing and minimizing banding artifacts. They are essential for professional photography and scientific research, where maintaining detail in highlights and shadows is crucial.

ImageJ, a popular image analysis tool, supports different bit depths, including 8-bit, 16-bit, and 32-bit float formats. These high bit depths are especially useful in scientific imaging for quantitative analysis, offering more accurate measurements and reducing noise. ImageJ provides tools for background subtraction, area and intensity measurements, and geometric transformations, making it a versatile tool for detailed image processing and analysis (Collins 2007). Bit depth in ImageJ is an essential feature that influences how images are analyzed and

processed. Understanding and managing bit depth is crucial for ensuring that images retain their quality and detail throughout various stages of imaging and analysis, particularly in scientific research and professional imaging. In ImageJ, bit depth refers to the number of bits used to represent the color or intensity of each pixel in an image. ImageJ supports various bit depths, which can affect how images are processed, analyzed, and visualized. Here's an overview of how bit depth works in ImageJ, including how to check and adjust it(Nagasaka et al 2017;Rueden et al 2017)

ImageJ supports several bit depths. In an 8bit depth each pixel represents 256 intensity levels (0-255) that is commonly used for grayscale images and simple color images. In a 16-bit depth each pixel represents 65,536 intensity levels (0-4095). This is ideal for scientific imaging, as it allows for more detailed data and less noise in the image. A 32-bit float is used for high dynamic range imaging and can represent a vast range of values, including decimals. This format is often used for advanced image processing and analysis.

High bit depth images (16-bit or 32-bit) are especially useful in scientific applications, such as Quantitative analysis for more accurate measurements due to greater intensity resolution and in image processing as Advanced technique that can be applied without degrading image quality (Gallagher, 2010).

1.5.1 Software settings

Before conducting the analysis of an image, it is essential to understand the relevant parameters and settings that are part of the process. This understanding facilitates the selection of optimal conditions that yield the most accurate results and aids in the interpretation of the data. Here, various parameters are employed, examining the advantages and disadvantages of the methods and each setting. The impact is studied, and an attempt is made to optimize the stain

quantification method. Since stain intensity is the desired measurement, the following parameters were considered.

1.5.2 Thresholding

Thresholding is an image processing technique that converts grayscale images into binary images based on intensity thresholds. Thresholding highlights regions of interest by setting pixel intensity ranges, enabling efficient analysis and measurement of objects. A threshold value (or range) is chosen to differentiate the foreground (objects) from the background. In a grayscale image, the total pixel intensity ranges from 0 (black) to 255 (white) for 8-bit images. Pixels with intensities above the threshold are typically considered foreground while those below are set to the background (or vice versa, depending on the application). After applying the wanted threshold, the image is usually converted to a binary black and white form. Foreground pixels are assigned one value (white or “1”), and background pixels are assigned another (black or “0”), making objects distinct from the background (Gonzalez and Richard., 2002).

Thresholding is widely used for object segmentation in isolating cells, tissues, or colonies from the background in ALP stained images, in particle size analysis for measuring size and distribution in microscopy, in feature separation for differentiating components like nuclei or blood vessels, for intensity-based filtering in analyzing stained regions in histological images, in morphometric analysis for extracting shape features like perimeter or circularity, in medical imaging for segmenting structures (e.g., bones, tumors) in CT, MRI, or X-rays in automated analysis for preprocessing large datasets in high-throughput workflows.

Manual thresholding and auto thresholding are two approaches to segmenting an image by converting grayscale values into binary images based on intensity levels. Manual Thresholding involves user selection of a specific intensity value to separate foreground from background. It is

suitable for images with high contrast or clear boundaries, offering direct control and precision, especially when dealing with images with uneven lighting or complex features with distinct pixel values that automatic algorithms might struggle to classify accurately. Manual thresholding allows researchers to accurately isolate stained colonies of pluripotent cells by adjusting the threshold to select stained areas, which is crucial in images with varied background lighting or staining intensity. Additionally, it enables tailored adjustments in cases of irregular colony morphology or background noise, leveraging user expertise for precise analysis. A higher threshold may facilitate the identification of more areas; however, it can also introduce excessive specks or noise. Manual Thresholding is time-consuming, prone to user bias, and less efficient for large datasets (Schneider et al 2012).

Automatic thresholding is more efficient for large datasets or high-throughput analysis, reduces subjectivity and user bias by automating the threshold selection process and can handle complex images with varying intensities or lighting conditions. Auto thresholding uses algorithms like Otsu's method, Yen, and adaptive thresholding to automatically determine the optimal threshold value for segmentation, often based on image properties such as histogram analysis. It is faster, more consistent, and efficient, especially for high-throughput analysis or images with complex conditions. However, it offers less control and may struggle with images with uneven contrast or overlapping intensities (Otsu 1979).

Automatic thresholding is ideal for processing large datasets with consistent foreground-background contrasts, whereas manual thresholding is better suited for fine-tuning specific images with irregular conditions.

1.5.3 Edge Processing

When processing images of stem cells stained for pluripotency markers like ALP, edge detection plays a vital role in two key analyses. Quantifying colony formation (i.e. analyzing edges) allows for accurate counting of colonies and colony size measurement, which is essential for assessing stem cell growth and viability. Morphological analysis (i.e. edge detection) evaluates the shape and spread of colonies, offering insights into the health and differentiation status of the stem cells. These analyses are crucial for understanding stem cell behavior and characteristics in research focused on pluripotency and differentiation. Undifferentiated colonies typically exhibit a round morphology, characterized by smooth and well-defined edges. These colonies are generally uniform in appearance and density. Their consistent shape and structure make it easier to use image processing techniques. In contrast, differentiated cells often display irregular or spiky morphologies. These shapes can be more complex, featuring protrusions, indentations, or uneven edges (Nagasaka et al 2017). The "Find Edges" filter identifies boundaries based on sharp changes in pixel intensity. By highlighting only the significant intensity changes, the algorithm reduces the impact of irrelevant details in the image. This method improves the differentiation of distinct morphological characteristics of the colonies while also mitigating noise and artifacts that could compromise subsequent thresholding operations (Russ and Neal, 2016).

1.5.4 Masking

Masking is a fundamental technique in image processing to isolate specific regions of interest within an image for detailed analysis. This method allows users to select and delineate areas based on criteria such as pixel intensity, color, or geometric shape. Masking effectively removes unwanted background noise, allowing researchers to focus on relevant features and thereby enhancing the clarity of subsequent analyses. Once regions are masked, a variety of

quantitative measurements can be performed on the isolated areas, including metrics related to area, intensity, and shape. This process typically involves thresholding to generating an image representing the specific features of interest, such as cellular colonies or other objects of study. The masked regions can be accessed and analyzed using the “Analyze Particles” function within ImageJ, followed by selecting the “Mask” option from the “Show” dropdown menu (Figure 1). The application of masks not only enables quantitative assessment; it also enhances the visualization of specific features within an image, making the analysis more comprehensible and robust. Through these capabilities, ImageJ masking serves as a valuable tool for researchers across various fields of study (Sheffield 2008).

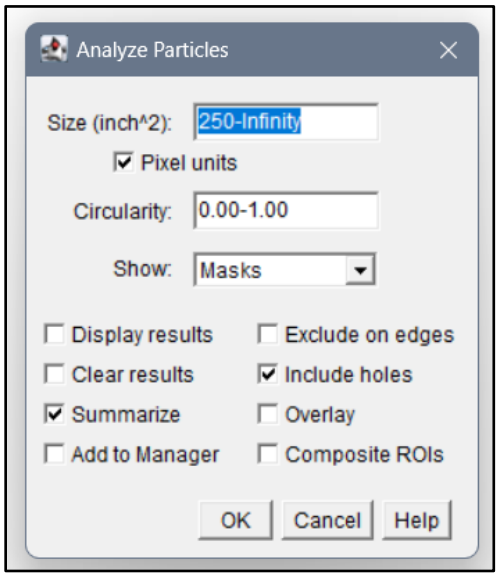

Figure 1: The mask of the measured colonies can be accessed by using the ‘analyze particle’ function.

1.5.5 Outline

Outlining particles is accessed via the "Analyze Particles" function of ImageJ. By selecting the "Outline" option from the "Show" dropdown menu, the software generates an 8-bit image that displays the outlines of measured colonies in a binary format. Each particle identified in the

image is delineated with a distinct outline, which is labeled and assigned specific gray levels. This functionality is instrumental for clearly visualizing the boundaries of measured particles, thereby enhancing the analysis of results and the presentation of data.

1.5.6 Holes Inclusion

In image processing, holes refer to gaps or empty regions within objects or segmented areas, which can affect the accuracy of analysis, especially in tasks like measuring morphology. These holes can be categorized into intra-object holes (holes within the object itself, a void inside a cell or colony), background holes (gaps in the background that may need to be addressed during segmentation) and artifacts (false holes caused by noise, improper thresholding, or incomplete segmentation).

Hole filling is essential for proper segmentation, ensuring that gaps within objects are treated as part of the object. This is important for tasks like colony counting or particle analysis. techniques for hole handling include morphological operations such as dilation, closing, and direct hole filling to remove or fill holes and post-processing to refine thresholded images for continuous, connected objects. Hole filling is crucial in biomedical imaging to maintain the integrity of analyses involving cell colonies, tissues, or particles. Proper handling ensures more accurate and reliable results (Stefkova et al 2015).

The “Include Holes “option in ImageJ which can be found under the analyze particle window was employed for all images. This feature allows the software to interpret the structure of particles in a binary image by determining whether to account for interior holes within those particles. When enabled, ImageJ recognizes interior holes as integral components of the particles. Consequently, the software identifies each particle by tracing its outer boundary, incorporating any enclosed areas (holes) as part of the same particle. This method demonstrated a degree of

reliability in the analysis of staining and morphological characteristics and was consequently chosen for the quantification of all images.

1.6 Goals of the Study

The zur Nieden lab has previously conducted an RNA sequencing study of stirred-suspension bioreactor cultivated human ESCs. In collaboration with the lab of Dr. Hideaki Tsutsui (Chemical Engineering, UCR) they have compared the resulting transcript profiles to cells grown in adherent conditions as well as cells that were aggregated, but not stirred. In that study, transcript signatures were found that suggested that the shear stress in the stirred environment is partially able to overcome aggregation-induced differentiation. Similarly, kinases and receptors associated with several signaling pathways were identified to be differentially regulated, potentially governing the observed changes. This led to the hypothesis that such signaling pathways may be manipulated to overcome the aggregation effect completely and yield naïve pluripotent colonies in stirred suspension, which brings the advantages listed above. Since bioreactors require relatively large culturing volumes, testing this hypothesis in stirred tanks is not financially feasible. Therefore, the **ultimate goal** of this study was to screen the identified chemical modulators in 2D cell culture plates for their effect on pluripotency.

To assess pluripotency in smaller scale settings, such as 48-well plates, a limited number of pluripotency assays exist, among them ALP stain. To quantitatively assess ALP activity, the **immediate goal** of this study was to develop a quantitative image-based analysis using ImageJ software. Quantitative analysis of colonies in image-based studies is critical for evaluating experimental outcomes in biological research. Accurate detection depends on effective thresholding and particle size settings to distinguish colonies from background noise. Manual thresholding, although precise, is subjective and time-intensive, while automatic thresholding

provides efficiency but may diminish under variable conditions. Additionally, the inclusion or exclusion of particle holes further complicates the analysis. This study aims to systematically evaluate these factors to optimize colony detection accuracy.

Therefore, the goal of the study is to develop an imaging analysis method with which we can assess pluripotency in cell cultures, on plates. Secondarily, the goal is to characterize the pluripotency in chemically manipulated cultures using this new method.

2 MATERIALS AND METHODS

2.1 Human Embryonic Stem Cells Culture Maintenance

Human embryonic stem cells of the H9 line (WiCell Research institute, Madison, WI, USA) were cultured according to previous protocols established and used within the zur Nieden lab (Madrid et al., 2023). The cells were viewed under an optical microscope (Nikon Eclipse 80i, Nikon Instruments, Melville, NY, USA) to assess morphology and confluency. Once they reached 60-80% confluency, typically within 3-4 days, they were passaged to a new well.

The wells were coated with Matrigel (BD Biosciences, San Diego, CA, USA), prepared using 14 mL of DMEM/F12 medium and 1 mL of Matrigel. The coated wells were incubated at 37°C with 5% CO_2 for 15 minutes. Then, 1 mL of mTeSR medium (Stem Cell Technologies, Seattle, WA, USA) was added to the Matrigel-coated wells.

In the old wells containing H9 cells, the supernatant was discarded, and the cells were washed twice with 1X phosphate-buffered saline (PBS). Accutase® was then added to facilitate enzymatic cell dissociation for 1 minute at room temperature. The Accutase® was carefully removed, and 1 mL of mTeSR medium (at room temperature) was added to each well. Cell scrapers were employed to physically detach the cells from the Matrigel.

The cell suspension was gently pipetted up and down to break the cell cluster into smaller aggregates and the colony size was checked under the microscope. The cell suspension was then added to new Matrigel-coated wells containing mTeSR medium, following a ratio based on confluency (the standard ratio for H9 cell passaging was 1:6 for 70% confluency). The culture plate was subsequently placed in an incubator at 37°C with 5% CO_2. Cells were checked daily under a microscope for growth and any potential contamination until they reached 60-80% confluency.

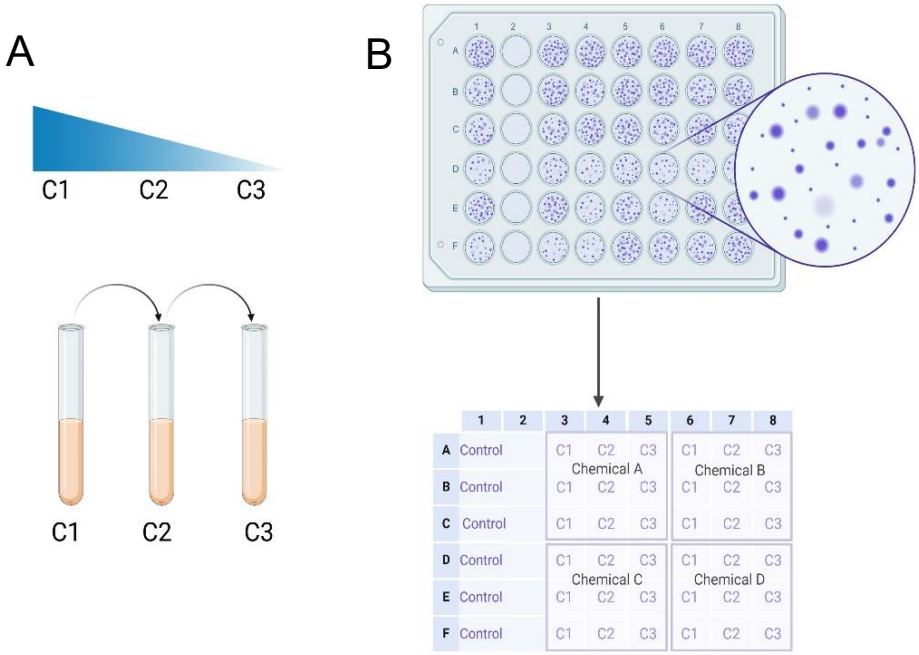

Figure 2: Schematic diagram of the chemical screening assay protocol: (A) Serial dilution and chemical media preparation, (B) Clump formation and Rocki plating setup. Created with Biorender.

2.2 Chemical Screening Assay

The plate-based chemical screening assay was conducted under two distinct culture conditions: aggregates of cell colonies or cell clusters (clumps) and single cells (ROCKi). The transition to single-cell culture was facilitated using a Rho-associated protein kinase inhibitor

(ROCKi) Y-27632. The assay included three concentrations of each chemical compound (C1, C2, and C3). Each concentration was replicated across three wells, resulting in a total of nine wells per chemical (3 concentrations × 3 trials) (Figure 2).

2.3 Chemical Media Preparation

Predilution stocks were prepared from the chemical stocks based on their IC50 values, utilizing two dilution schemes: 1:5 and 1:10. From these predilutions, C1 was established, followed by C2 and C3 through serial dilution, with C1 representing the highest concentration and C3 the lowest (Figure 2A). The chemical media were prepared based on the concentrations specified in Table 1.

In the 1:5 dilution series, 1600 µL of mTeSR was added to each of the three designated tubes. Following this, 400 µL of the predilution was introduced into each tube. The tubes were then capped, inverted, and mixed thoroughly. To create C2, 400 µL was transferred from the first tube (C1) to the second tube (C2), which was subsequently mixed. Finally, 400 µL from C2 was transferred to the third tube (C3), followed by thorough mixing.

Table 1: Concentrations used for chemical media preparation

TARGET	CHEMICAL NAME	C1	C2	C3
p38MAPKa	Asiatic Acid	1 µM	5 µM	25 µM
I3Ka	740 Y-P TFA	2 µg/ml	10 µg/ml	50 µg/ml
IGF1Ri	BMS-536924	1 µM	0.1 µM	0.01 µM
IGF1Ri	Linsitinib (OSI-906)	0.16 µM	0.8 µM	4 µM
CK1αi	Epiblastin A	0.4 µM	2 µM	10 µM
SHP2i	LY6	2 µM	10 µM	50 µM
IRS1a	Insulin	1 nM	5 nM	25 nM
LKB1a	TMPA	4 µM	20 µM	100 µM
PDGFRba	PDGF-BB	1 ng/ml	5 ng/ml	25 ng/ml
JNKi	JNK-IN-8	1 nM	5 nM	25 nM
EGFRi	Icotinib	1 nM	5 nM	25 nM
PKC	PKC-IN-1	8 nM	80 nM	800 nM
PKCεi	Epsilon-V1-2	0.2 µM	1 µM	5 µM
PDK1i	MP7	0.2 µM	1 µM	5 µM
FAKi	Y15	0.2 µM	2 µM	20 µM
FAKi	YH-306	2 µM	10 µM	25 µM
TAK1a	TGFbeta-1	100 pg/ml	1 ng/ml	10 ng/ml
TGFbi	LY2157299 monohydrate	2 nM	10 nM	50 nM
TGFbi	GW788388	0.2 µM	1 µM	20 µM
PAK1i	NVS-PAK1-1	0.4 µM	2 µM	10 µM
PAK1i	G-5555	1 µM	5 µM	20 µM
IGF1Ra	IGF1	25 ng/ml	5 ng/ml	1 ng/ml
CK1αa	SSTC3	100 nM	30 nM	10 nM
LKB1i	Pim1/AKK1-IN-1	3 µM	1 µM	0.3 µM
EGFRa	NSC228155	10 µM	3 µM	1 µM
PKCεa	PMA	10 µM	3 µM	1 µM
PKCεi	Sotrastaurin	10 nM	3 nM	1 nM
TAK1i	Takinib	30 nM	10 nM	3 nM

2.4 Clump Method

As previously described, H9 cells were split in a 1:6 ratio into 48 well plates once 70% confluence was reached. A total of 250 µL of the prepared cell suspension was added to each well. Subsequently, 250 µL of the corresponding chemical media (C1, C2, or C3) was introduced to each well, yielding a total volume of 500 µL per well. Control wells were prepared by adding 250 µL of

cell suspension and 250 µL of mTeSR medium. Cells were monitored daily for growth and morphological changes throughout the experimental period. Once cells reached 60-80% confluency, typically after three days, they were fixed and subjected to staining for subsequent analysis.

2.5 ROCKi Method

The H9 cells were pretreated with 10 µM ROCK inhibitor (ROCKi) in mTeSR1 medium for 1 hour. Following pretreatment, the media was aspirated, and the cells were rinsed three times with phosphate-buffered saline (PBS) containing magnesium (Mg^{2+}) and calcium (Ca^{2+}) ions (PBS -Mg^{2+} -Ca^{2+}). Subsequently, cells were treated with pre-warmed 0.25% Trypsin-EDTA solution at 37 °C for 5 minutes, with a volume of 1 mL per well in a six-well plate. Neutralization of trypsin was achieved by adding an equal volume of medium-containing cell suspension. The cell suspension was transferred to a conical tube containing a 50% fetal bovine serum (FBS) and Dulbecco's Modified Eagle Medium (DMEM) mixture, maintaining a 1:1 ratio (e.g., 1 mL of Trypsin, 1 mL of FBS, and 1 mL of DMEM per well) and was centrifuged at 1200 rpm for 5 minutes. Subsequently, the supernatant was carefully aspirated, and the cell pellet was resuspended in an appropriate volume of 10 µM ROCKi in the ratio of 1:1000 of mTeSR1 medium. To achieve a single-cell suspension, the cells were gently triturated using a 1000 µL pipette approximately 15-20 times. The cells were then counted using a hemocytometer. Following cell counting, approximately 1,467 cells were seeded in mTeSR1 medium containing 10 µM ROCKi into wells of a Matrigel-coated 48-well plate. Subsequently, 250 µL of the corresponding chemical media (C1, C2, or C3) was introduced to each well, yielding a total volume of 500 µL per well. The medium was changed to mTeSR1 without ROCKi 24 hours post-seeding. Control wells were treated with 250 µL of cell suspension and 250 µL of mTeSR medium. Cells were monitored daily for growth and morphological changes

throughout the experimental period. Once cells reached 60-80% confluency they were fixed and subjected to staining for subsequent analysis.

2.6 Alkaline Phosphatase (AP) Staining

After 4 days of culture, the medium was carefully aspirated from all 48 wells, and cells were washed with 1 mL of 1X phosphate-buffered saline with Tween PBST (1X PBS containing 0.05% Tween-20). Following this, the wash solution was aspirated. The fixing solution (supplied with the staining kit) was added and incubated at room temperature for 2 minutes. After incubation, the fixing solution was removed, and the fixed cells were washed twice with 1 mL of 1X PBST. Alkaline phosphatase (AP) staining solution was added to each well, and the cells were incubated at room temperature for 15 to 30 minutes in the dark to protect from light exposure. Upon completion of the incubation period, the AP staining solution was aspirated, and the stained cells were washed twice with 1 mL of 1X phosphate-buffered saline (PBS). The cells were then stored in 1X PBS at 4°C for long-term preservation while the cells overlaid with 1X PBS containing 20% glycerol and maintained at 4°C.

2.7 Statistical Analysis

A one-way ANOVA to assess the differences between the various concentrations and the control group was conducted. The analysis was performed using GraphPad Prism software (v9.2., GraphPad Software Inc., San Diego, CA, USA). P-values less than 0.05 were deemed significant.

3 RESULTS

The cells were exposed to chemicals in a 48-well plate for a chemical screening assay. The colonies were stained with alkaline phosphatase stain when the cells reached 60-80% confluence, typically after 3 days for clump conditions and 4 days for ROCKi conditions. Visual observation of

colonies utilizing a microscope, such as the Echo Revolve microscope, allows for the preliminary assessment of the effects of various chemicals. However, this method alone is insufficient for a comprehensive analysis. Incorporating computerized image analysis provides a more reliable and quantitative evaluation of the observed results, thereby enhancing the accuracy of the conclusions drawn from the study.

To differentiate between differentiated and undifferentiated colonies, various methods to assess stain intensity and morphology from images were employed. Each method has its advantages and disadvantages. For instance, some methods may provide clearer visualization and require more complex procedures, while others are simpler and less precise.

In this study, we selected a method that demonstrated a significant difference in stain intensity and effectively identifies the morphological differences between differentiated and undifferentiated cells. This approach enhanced our understanding of the effects of the chemicals on cell differentiation, facilitating accurate classification. Below is an outline of steps taken to develop the image analysis approach and reach the ultimate goal of quantitatively assessing the effect of selected chemical modulators on pluripotency.

3.1 Quantification of ALP using Image J

3.1.1 Method I: Edge Detection Method

The study was to visualize the edges effectively before applying thresholding to isolate the colonies and to study the morphology of the undifferentiated and differentiated colonies. This method employed a series of systematic steps for image processing and analysis as shown in the figure below. Initially, input TIFF images were converted to an 8-bit grayscale format, creating a duplicate grayscale image for further processing.

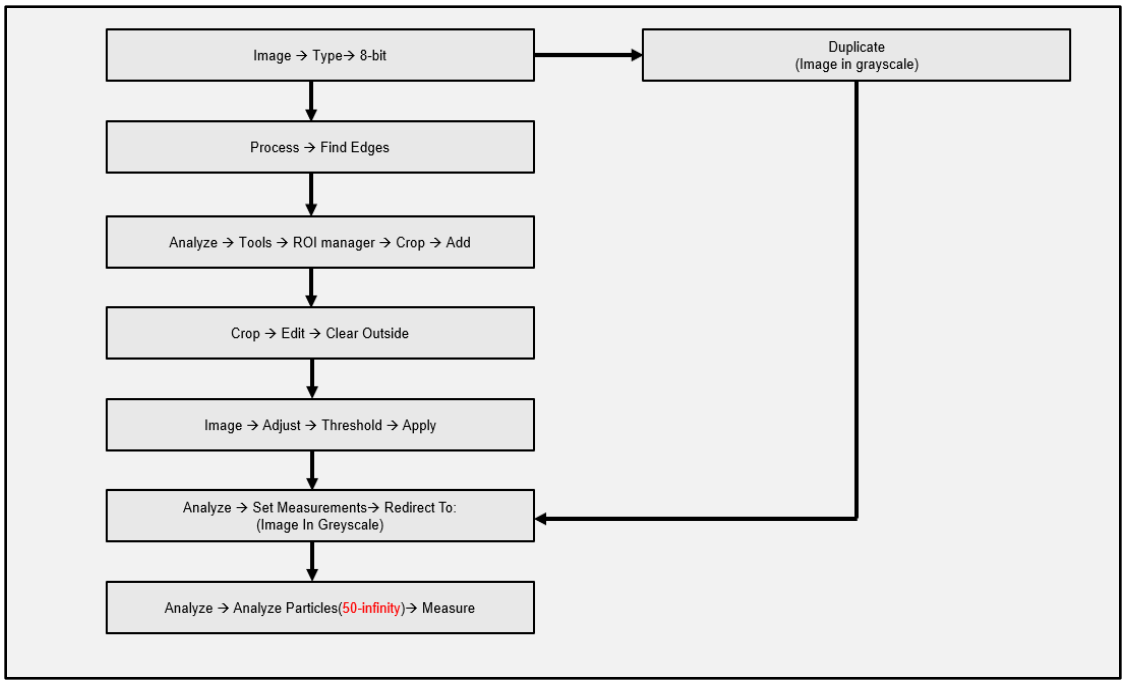

Figure 3: Flowchart of Method 1- Edge Processing for Morphological Analysis.

Edge detection was performed using the "Find Edges" function, resulting in an image that highlighted the edges of the colonies. The image was then automatically thresholded to optimize the coverage of the colonies and ensure that the majority of them were distinctly marked in red. Following the thresholding process, the image was converted into a binary format.

The Region of Interest (ROI) Manager was used to define a circular selection with a consistent diameter of 2790 pixels across all images. The "Clear Outside" command removed data outside this circular area. Before analysis, the cropped binary image was redirected to its original grayscale version.

The cropped images were then analyzed using the "Analyze Particles" command. The size range for included particles varied based on the particulate characteristics of the images, set between 50 pixels and infinity or from 1500 pixels to infinity, to exclude debris below the specified thresholds. The “Redirect to” pull-down menu was used to choose the relevant image as reference for analysis (Stossi et al 2023) (**Figure 3**). When measuring data, it is crucial to select the appropriate image to ensure accurate results. Finally, relevant quantitative data were extracted from the measurements taken from the images (**Figure 4**).

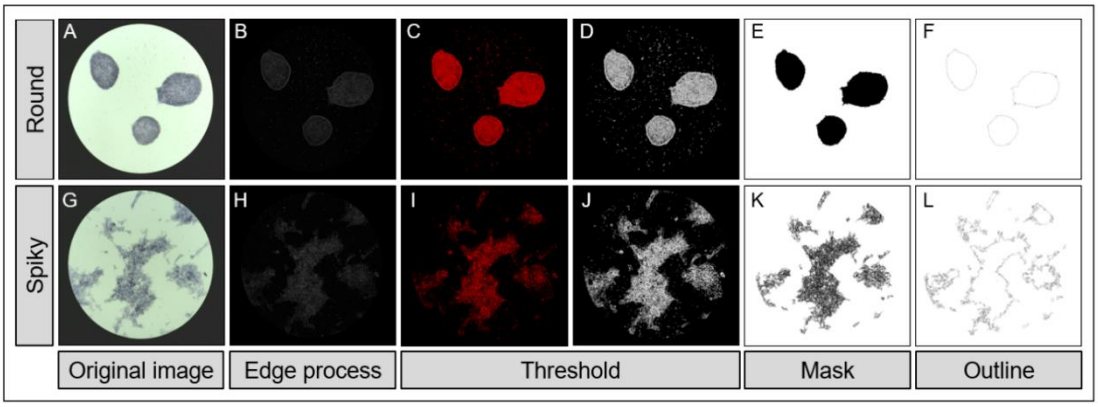

Figure 4: Edge Detection Method for Morphology Analysis. (A, G) Original TIFF image representing round and spiky colonies. (B, H) Image after applying the Find Edges filter. (C, I) Image with adjusted threshold, highlighting areas of interest in red. (D, J) A binary image is created after applying the threshold. (E, K) Mask of the measured colonies. (F, L) Outlines of the measured colonies.

Despite the application of "Find Edges," there were challenges in fully highlighting the colonies. The darker parts of the colonies were not adequately detected or highlighted during the thresholding process. This issue suggested that the intensity values of these darker regions were

not significantly different from their background, making them less likely to be recognized as edges. After applying the "Find Edges," thresholding was performed to delineate the colonies further. Both round and spiky colonies yielded similar values, which could hinder the differentiation of morphological features indicating that the edge process may not have been sensitive enough to capture the unique characteristics of the spiky morphology, leading to a loss of detail necessary for accurate analysis.

3.1.2 Method II: Image Subtraction Method

When culture plates are fixed and stained, a common issue encountered is the presence of debris, stain particles, and dead single-cells that remain even after washing with PBS. These unwanted particles can complicate the analysis, as they may be misidentified as colonies during the thresholding step. This misidentification can adversely affect the quantification of stain intensity by skewing the mean values. The presence of dead single cells, which typically appear circular, can artificially inflate the mean circularity measurements, leading to inaccurate assessments.

A method was employed to remove artifacts, enabling accurate measurement of viable colonies and minimizing debris interference to improve the reliability of quantitative analyses.

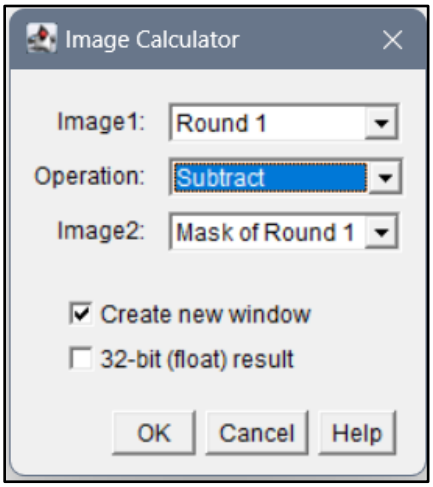

Figure 5: Image calculator dialog box displaying the thresholded image "Image1" (saved as "Round1") and the debris mask "Image2" (saved as "Mask of Round 1").

The subtraction command facilitates the removal of one image from another, thereby enabling the isolation of specific features, such as colonies from debris. This process can be executed by navigating to the command: Process > Image Calculator. Following the analysis of particles, a mask will be generated that highlights the debris. This binary mask, characterized by white pixels representing debris and black pixels representing the background, will serve as the basis for subtraction. The "Subtract" operation is selected to remove the debris mask from the thresholded image (**Figure 5**).

The initial steps of this method are consistent with those of the previous approach, involving the conversion of the image to an 8-bit format, followed by edge processing, thresholding, and masking. In the final steps, a mask specifically for debris and artifacts is generated by adjusting the circularity value during the analyze particle step. Given that debris and artifacts typically exhibit smaller and more circular characteristics compared to the actual colonies, a mask isolating only the debris can be achieved by setting a circularity value between

0.25 and 1.00 in pixel units. Subsequently, this debris mask is subtracted from the thresholded image, resulting in a mask that primarily contains only the colonies (**Figure 6**).

The resultant image will exclusively display the colonies, with areas previously occupied by debris rendered black (or zeroed out), thereby providing a clear representation of the colonies (**Figure 7**).

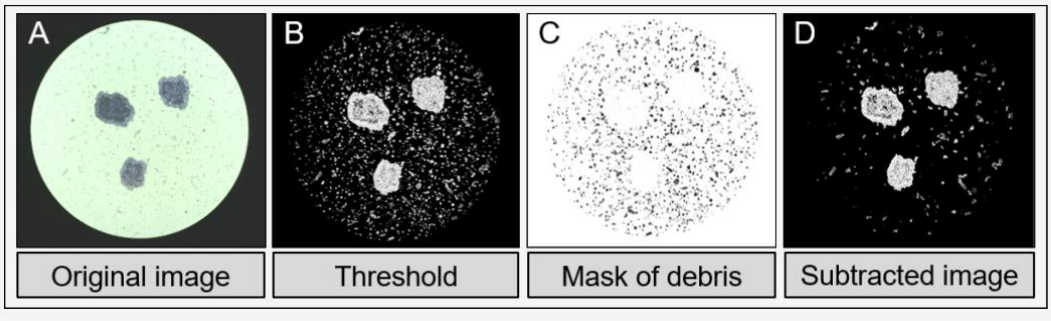

Figure 6: Flowchart of Method 2: Image Subtraction for Debris and Noise Reduction.

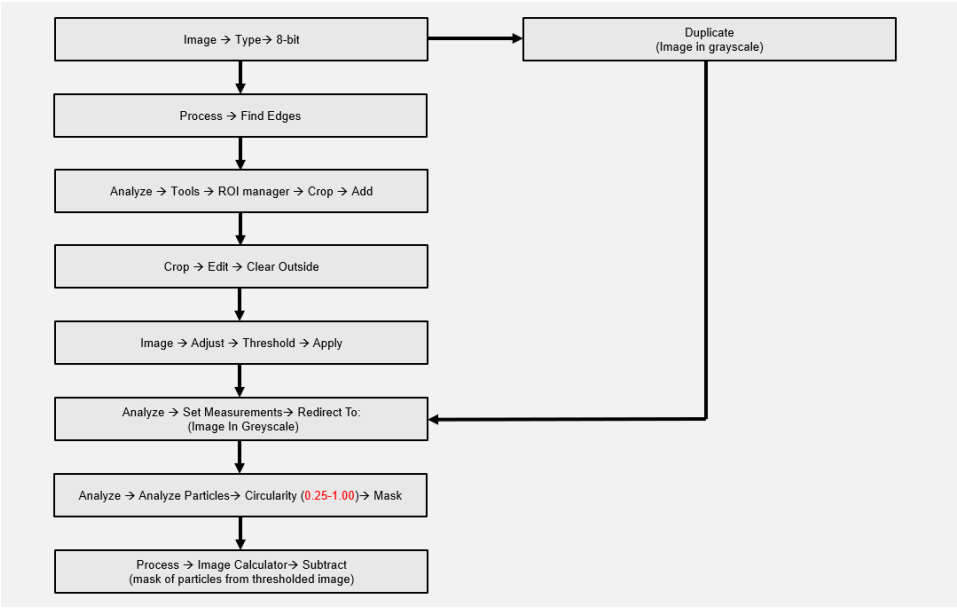

Figure 7: Image subtraction method for debris and noise reduction. (a) Original TIFF image of round colonies. (b) Thresholded image. (c) Mask of debris and noise to be removed. (d) Resultant image after subtraction, displaying the colonies.

This method operation effectively subtracted the pixel values of the debris mask from the image of the colonies and eliminated noise or artifacts that may arise during thresholding. This

method presented several advantages; however, it was crucial to accurately define the debris mask. Failure to do so resulted in the unintended removal of portions of the colonies, consequently leading to the loss of valuable data. Selecting appropriate thresholds for both the colonies and the debris can be challenging and may require multiple adjustments. Inaccurate thresholding can result in either incomplete removal of debris or the loss of important colony details. Furthermore, reliance on circularity as a parameter may not adequately include all types of debris, particularly those exhibiting irregular shapes.

3.1.3 Method III: Standard Stain Quantification and Morphological Analysis

This method represented a modification of the procedures discussed in the publication by Bolte et al (2006). The initial steps of this method are consistent with those described earlier. They involve generating a binary image and creating a duplicate to serve as the reference image in the final phase of the procedure **(Figure 8**).

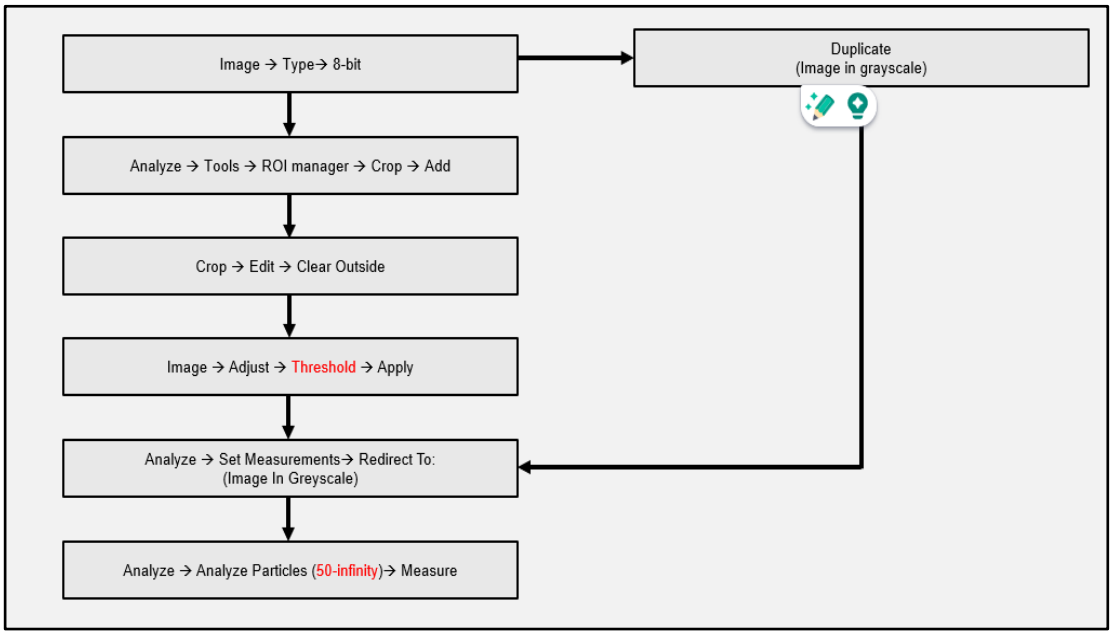

Figure 8: Flowchart of Method 3: Standard Stain Analysis method for Stain Quantification and Morphological Analysis.

In this method, the threshold can be manually and automatically adjusted to encompass the entire area of interest for stain quantification, specifically focusing on the colonies while eliminating unwanted debris and artifacts from the thresholding process. Any artifacts generated during the thresholding step are subsequently removed in the analyze particles section by defining the pixel size for analysis, which varies for each image (1000-40000). For the analysis of colonies, the thresholded image is redirected to the input image (grayscale), replacing black masks with shaded masks based on the intensity of the input image **(Figure 9**).

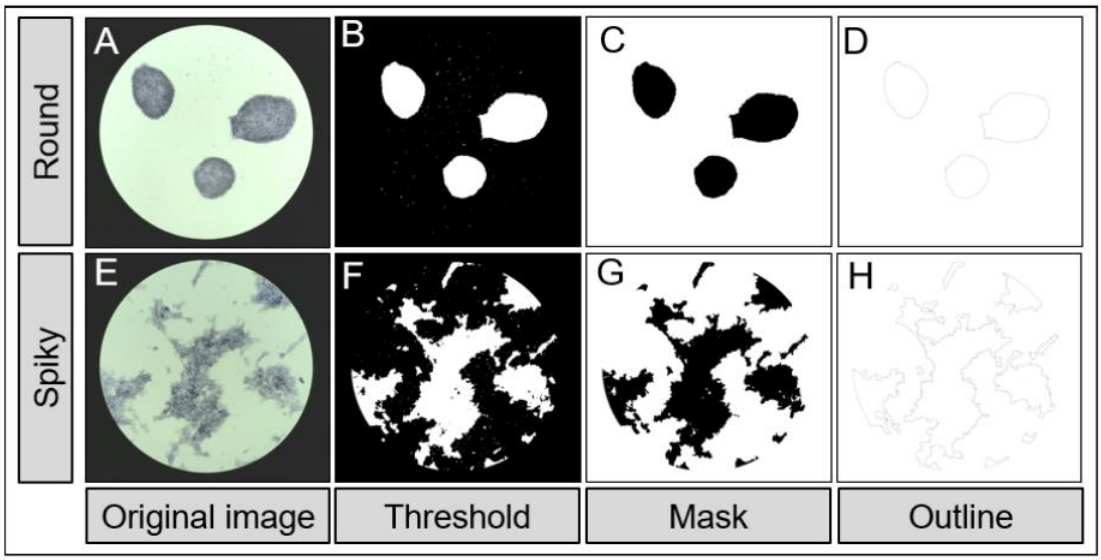

Figure 9: Method Optimization for Stain Quantification Morphological Analysis (a) Original TIFF image of round and spiky colonies(representative). (b) Thresholded image. (c) Mask of the measured colonies. (d) Outlines of the measured colonies.

One of the notable limitations of this method was its inability to detect lightly stained colonies or areas within colonies where staining is insufficient during the thresholding process, which typically occurs at the centers of larger colonies and spiky fragments of differentiated colonies. When lightly stained areas of colonies were not detected during thresholding, it resulted

in incomplete representation of the colonies leading to underestimation of colony counts and potentially obscuring important phenotypic variations within the sample. This lack of sensitivity may adversely affect parameters such as area fraction, circularity, mean gray value, and other relevant metrics. To address this issue, the "Include Holes" option in ImageJ which can be found under the analyze particle window was employed for all images. This feature allowed the software to interpret the structure of particles in a binary image by determining whether to account for interior holes within those particles. When enabled, ImageJ recognizes interior holes as integral components of the particles. Consequently, the software identified each particle by tracing its outer boundary.

3.1.4 Method III Optimization

This study further examined the effects of manual and automatic thresholding, particle inclusion sizes, and hole inclusion/exclusion on colony detection accuracy. Systematic experimentation was performed using five threshold settings (automatic and specific ranges) and particle inclusion sizes ranging from 5000 to 40000 pixels. The results demonstrated the impact of these parameters on noise reduction, colony differentiation, and detection accuracy, providing a robust framework for improving colony analysis workflows.

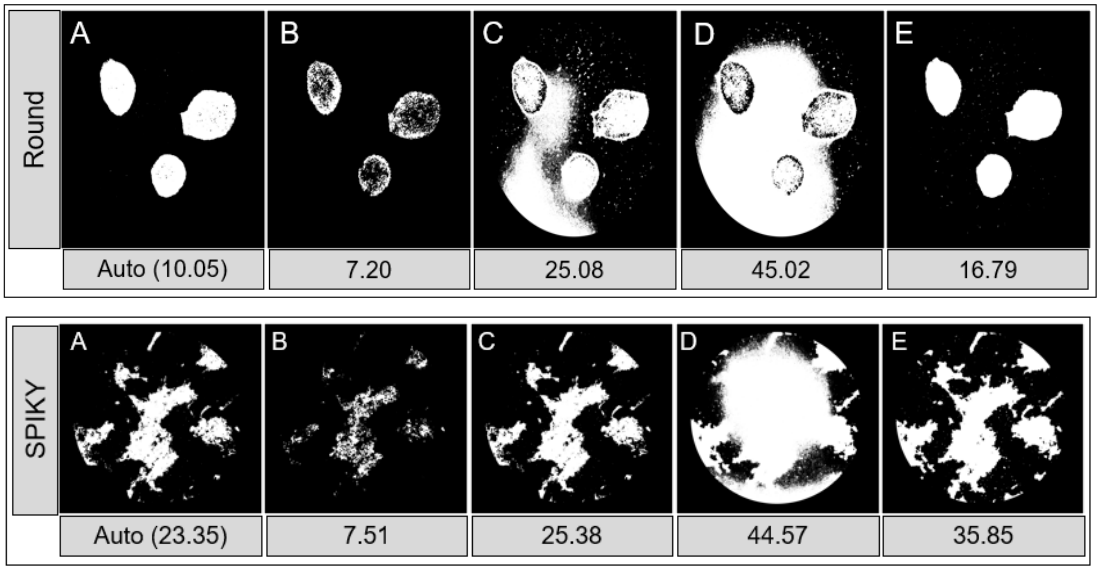

Figure 10: Representative image showing round colonies with varying threshold values. The threshold settings are as follows (a)automatic threshold (b)a very low threshold (c)moderate threshold (d)higher threshold.

Various thresholding and particle inclusion size settings were experimented to determine their effects on the data and how they impact the accuracy of colony detection. The goal here was to determine how different thresholding values (both manual and automatic) would affect the analysis and how these values relate to colony detection accuracy. Several trials were conducted to assess the influence of various threshold settings and particle inclusion sizes on the data. Five distinct threshold values were employed in the experiment, including automatic thresholding. These values were categorized as follows: a threshold range of 7 was considered a very low threshold, a range of 25 represented a moderate threshold, and a range of 45 indicated a high threshold.

Five different particle inclusion sizes were also tested, ranging from small to large (5000, 10000, 20000, 30000, and 40000). These sizes determine the minimum size of particles that the software will include as valid colonies.

Figure 10 shows how the thresholding beyond certain ranges adds more noise or causes particles to be falsely identified as colonies, leading to incorrect values. When the threshold is too high, the software might exclude smaller colonies or other features of interest, while including too many small debris or noise. If the threshold is too low, it might include too many irrelevant particles, increasing the chance of false positives. The figures and graphs help illustrate the differences between a true value threshold (the one that accurately captures the colonies of interest) and automatic thresholding values.

The graphs in Figure 11 highlight how automatic and manual thresholds influence data accuracy. The deviation from the actual threshold (true value) is highlighted, with the green bar representing round images and the blue bar representing spiky representative images.

i. Thresholding Analysis

Automatic Thresholding provided consistent but suboptimal results when image conditions varied. Low Threshold (7) overestimated colony areas, capturing noise and irrelevant particles. Moderate Threshold (25) balanced noise reduction and colony detection but failed to exclude some unwanted particles. The High Threshold (45) excluded most noise but occasionally omitted smaller colonies. Optimized Threshold delivered the most accurate results by tailoring settings to specific image features.

ii. Particle Inclusion Size Analysis

Smaller sizes (5000, 10000 pixels) detected noise and debris as colonies. Intermediate size (20000 pixels) achieved a balance between sensitivity and specificity. Larger sizes (30000, 40000 pixels): missed smaller colonies, reducing detection accuracy.

iii. Hole Inclusion Analysis

Including holes accurately identified hollow colonies, aiding morphological analysis whereas excluding holes simplified solid colony detection but misclassified hollow colonies.

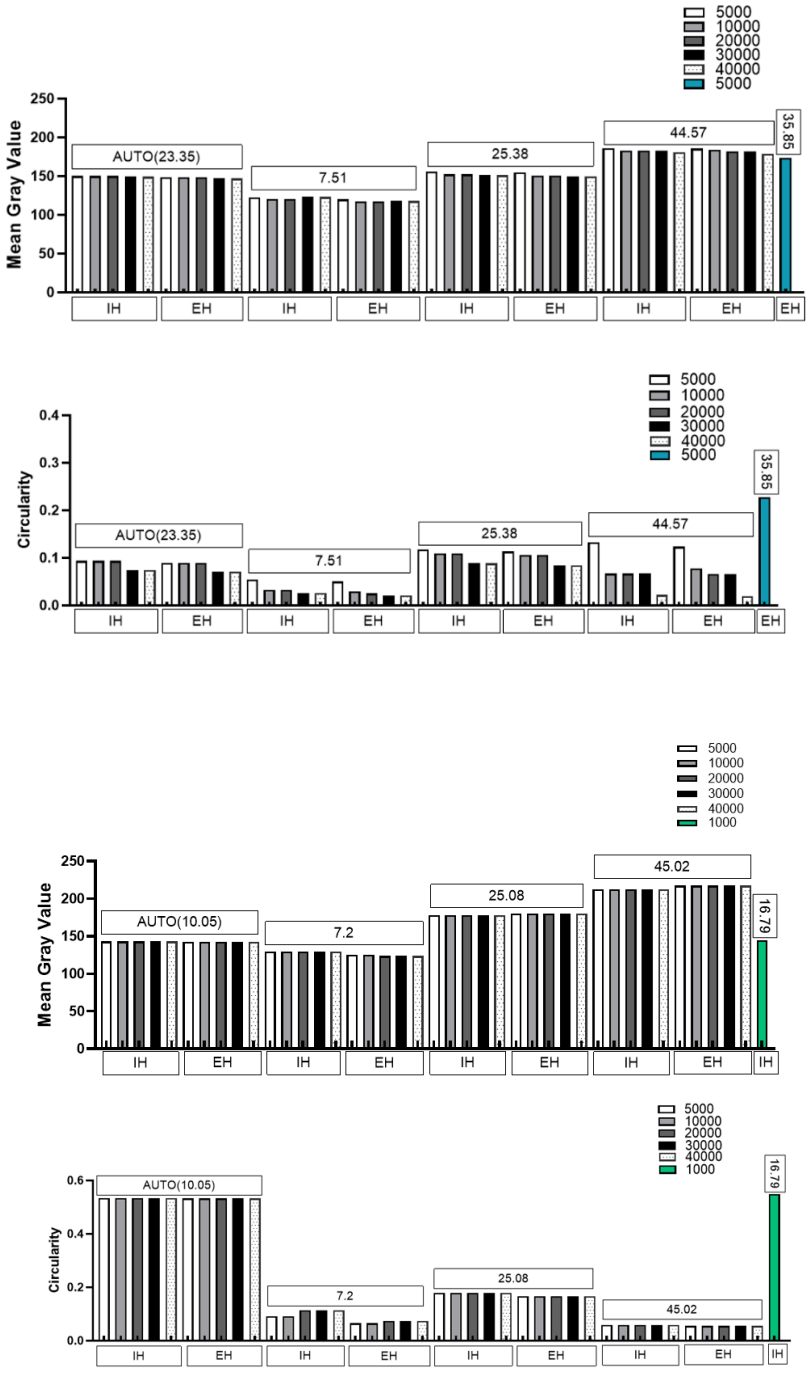

Figure 11: Graph showing the relationship between mean gray value and circularity for different particle inclusion sizes and thresholds. Green bars represent the true values for round colonies, while blue bars represent true values for spiky colonies.

3.2 Data Measurement

At the end of the analysis several endpoint measures are listed by the software. These shall be explained below.

i. Mean Gray Value (Stain Intensity)

Lower mean gray values correspond to darker-stained colonies, which typically indicate higher levels of alkaline phosphatase (ALP) marker expression and, consequently, greater pluripotency. Conversely, lighter-stained colonies, indicative of differentiation, display higher mean gray values.

ii. Circularity

This shape descriptor quantifies how closely a colony's shape resembles a perfect circle, with values ranging from 0 to 1. Higher circularity values suggest uniform and compact colonies, typically associated with undifferentiated states. Lower values indicate irregular or fragmented shapes, which may correspond to differentiation or morphological changes due to environmental factors.

iii. Area Fraction

This metric represents the proportion of the image occupied by colonies. Higher area fractions correlate with increased proliferation or colony density, while lower fractions may signify slower proliferation rates or cell death.

iv. Normalized Intensity

Data normalization was achieved by dividing the mean gray value by circularity, allowing for a composite metric that reduces shape-related biases. This approach enhances the accuracy of comparisons by integrating both intensity and shape features into a single value, providing a nuanced analysis of colony characteristics.

3.3 Effect of Chemicals

Twenty-one chemicals were originally identified from the RNA sequencing and protein microarray experiments previously conducted and the resulting images of the cell screen analyzed according to the optimized method 3 developed above. Representative images and resulting graphs for the mean grey value, circularity and normalized intensity are charted in the appendix and summarized in Table 2.

↑	Increased PP
↔	Maintained or no effect
↓	Decreased/Toxic

TARGET	CHEMICAL NAME	Expected Effect	CONDITION	Sample Size	Observed effect	Concentration
p38MAPKa	Asiatic Acid	↑	CLUMP	9	↑	All
			ROCKi	10	↔	C1
PI3Ka	740 Y-P TFA	↑	CLUMP	7	↑	C3
			ROCKi	7	↔	C2
IGF1Ri	BMS-536924	↓	CLUMP	10	↔	-
			ROCKi	10	↔	-
IGF1Ri	Linsitinib (OSI-906)	↓	CLUMP	8	↔	C3
			ROCKi	7	↔	C2
CK1αi	Epiblastin A	↓	CLUMP	7	↑	C2
			ROCKi	7	↔	C2
SHP2i	LY6	↓	CLUMP	9	↑	C3
			ROCKi	10	↔	C1,C2
IRS1a	Insulin	↓	CLUMP	7	↑	C3
			ROCKi	7	↑	C1
LKB1a	TMPA	↓	CLUMP	7	↔	C3
			ROCKi	6	↔	C3
PDGFRba	PDGF-BB	↓	CLUMP	10	↑	C3
			ROCKi	8	↔	-
JNKi	JNK-IN-8	↓	CLUMP	7	↔	C1
			ROCKi	8	↔	-
EGFRi	Icotinib	↓	CLUMP	8	↑	C1
			ROCKi	8	↔	-
PKC	PKC-IN-1	↓	CLUMP	7	↔	-
			ROCKi	8	↔	-
PKCεi	Epsilon-V1-2	↓	CLUMP	10	↑	C3
			ROCKi	10	↑	C2
PDK1i	MP7	↓	CLUMP	10	↔	C3
			ROCKi	10	↔	C3
FAKi	Y15	↑	CLUMP	7	↑	C2
			ROCKi	7	↔	C2
FAKi	YH-306	↑	CLUMP	8	↔	-
			ROCKi	8	↔	-
TAK1a	TGFbeta-1	↓	CLUMP	10	↔	
			ROCKi	8	↔	
TGFbi	LY2157299 monohydrate	↑	CLUMP	9	↔	C2
			ROCKi	10	↔	
TGFbi	GW788388	↑	CLUMP	10	↑	C3
			ROCKi	9	↑	C3
PAK1i	NVS-PAK1-1	↑	CLUMP	10	↓	-
			ROCKi	7	↓	-
PAK1i	G-5555	↑	CLUMP	7	↔	C3
			ROCKi	7	↔	C3
IGF1Ra	IGF1	↑	CLUMP	8	↑	C1,C3
			ROCKi	7	↔	C1,C3
CK1αa	SSTC3	↑	CLUMP	7	↓	C1
			ROCKi	7	↓	-
LKB1i	Pim1/AKK1-IN-1	↑	CLUMP	6	↔	
			ROCKi	7	↑	C2
EGFRa	NSC228155	↑	CLUMP	N/A	↓	-
			ROCKi	N/A	↓	-
PKCεa	PMA (Phorbol 12-myristate 13-acetate)	↓	CLUMP	N/A	↓	-
			ROCKi	N/A	↓	-
PKCεi	Sotrastaurin	↑	CLUMP	7	↔	C1
			ROCKi	7	↔	C1
TAK1i	Takinib	↑	CLUMP	7	↑	C1
			ROCKi	7	↑	C1,C2

Table 2: Summary of the results for all chemicals, including their target molecules, experimental conditions (Clump or Rocki), expected effects, observed results based on image analysis and statistical analysis, and the concentrations of the chemicals that showed significant effects.

This table also lists the names of the chemicals alongside their target molecules. The expected effects are derived from previously conducted protein array experiments and literature review. The observed results are based on image analysis and statistical evaluation using one-way ANOVA. The sample size corresponds to the number of images analyzed per chemical, while the concentrations represent the levels that effectively maintained pluripotency according to the One-Way ANOVA test.

Each chemical was compared with their respective untreated controls. In sum, chemicals such as Asiatic Acid, 740 YP TFA, Y15, YH306, and TGF-β inhibitors, including LY2157299 and GG788388, were hypothesized to enhance pluripotency. Image analysis of the observed data indeed indicated an increase in pluripotency, particularly under the clump condition. However, although YH306 did not show a noticeable increase in pluripotency, it also did not result in a decrease; rather, it appeared to help maintain pluripotency. On the other hand, chemicals such as NVS-PASK1-1, which were expected to support the maintenance of pluripotency, proved to be toxic.

A second round of chemical screening was then conducted using seven additional chemicals with decreased pluripotency as expected. In this second round, the chemical was switched to achieve the opposite from before. For example, the TAK activator TGF-β was expected to decrease pluripotency (and image analysis suggested no increase), a chemical inhibitor to TAK1, Takinib, was used to manipulate the activation state of this specific signaling pathway in the second round, where it was expected to show improvements in pluripotency. Among the chemicals tested, the Takinib compound indeed demonstrated a clear enhancement in pluripotency both in clump and ROCKi conditions, as anticipated. However, some chemicals, such

as NSC228155 and SSTC3, were unfortunately found to be toxic and their concentrations might need to be reduced in subsequent testing to prevent cell death.

3.5. Potential Chemical Combinations

The plate-based chemical screening assay, coupled with image analysis and statistical evaluation, allowed us to identify potential targets and assess the effects of various chemicals on pluripotency. This approach facilitated the identification of potential chemical combinations **(Figure 12)** that could help maintain pluripotency in a bioreactor environment.

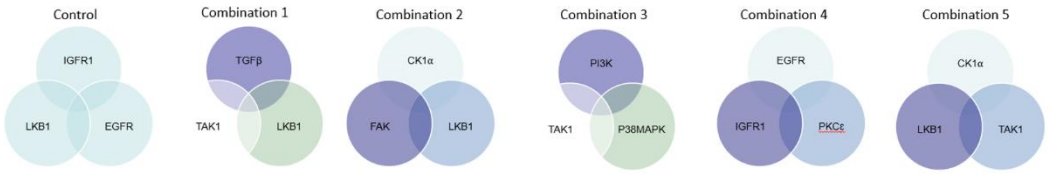

Figure 12: Potential combinations of chemicals.

4 DISCUSSION

In this study, a plate-based chemical screening assay was conducted to evaluate both activators and inhibitors of critical pathways associated with pluripotency including MAPK, TGF-β, IGF, and PI3 kinase that play roles in either inducing or suppressing differentiation (Brons et al. 2007). The cells were tested in a single-celled environment created using ROCK inhibitor (ROCKi) as well as in the environment where cells were allowed to proliferate and form colonies. To effectively visualize and differentiate between undifferentiated and differentiated colonies, AP staining procedures were employed. The purple-stained cell colonies from AP staining, indicative of undifferentiated ESCs, were enumerated in contrast to the colorless or lightly stained colonies, which represented differentiated ESCs, using a light microscope (Bolte and Cordelieres 2006;

Martello 2014) and a method developed here to analyze pluripotency from images of ALP-stained cell colonies. This chapter will discuss the advantages and disadvantages of image analysis followed by a discussion of the signaling pathways studied herein in the context of the results obtained.

4.1 Application of Image J

The application of ImageJ in chemical screening of pluripotency offers significant advantages in stem cell research, especially when evaluating the impact of various compounds on stem cell behavior. This powerful image processing software has proven to be a highly efficient tool for the quantitative assessment of pluripotency-related parameters, making it an invaluable asset in both high-throughput and detailed stem cell studies (Blauwkamp et al 2012).

One of the primary strengths of ImageJ is its ability to perform automated, quantitative analysis of cell morphology. Pluripotent stem cells exhibit distinctive morphological characteristics, such as compact colonies with clear boundaries, specific cell shapes, and sizes that differ from differentiated cells. By analyzing these features, ImageJ enables the identification of compounds that may influence pluripotency. For instance, compounds that promote differentiation often led to changes in cell shape, colony structure, and size (Katarzyna et al 2023). In this study, we successfully utilized ImageJ to differentiate between pluripotent and differentiated cells based on these morphological changes, thus identifying chemical compounds that either support or inhibit stem cell self-renewal. This capability of ImageJ to discern subtle morphological alterations allows researchers to gain insights into the biological effects of treatments on pluripotency (Yu Jin Zhang 2001).

Another key feature of ImageJ is its ability to assess cell proliferation and viability, which are critical metrics for understanding the impact of chemical treatments on stem cell growth. By

using assays such as viability dyes and proliferation markers, ImageJ allowed us to quantify the effects of chemical compounds on cell survival and division. The analysis revealed compounds that induced significant changes in cell proliferation, either by promoting or inhibiting growth. For instance, compounds that inhibit proliferation may drive differentiation or maintain cells in a more quiescent state, while others might stimulate cell expansion, which is important for therapeutic applications. Understanding these proliferation dynamics is essential for optimizing culture conditions and chemical treatments in pluripotent stem cell research (Tesar et al., 2007).

The ability of ImageJ to analyze time-lapse and dynamic imaging data adds an additional layer of insight into how chemical treatments influence stem cell behavior over time. By tracking changes in colony size, morphology, and movement, researchers can observe real-time effects of compounds on pluripotency. This dynamic capability helps to identify compounds that have a sustained effect on stem cell cultures, allowing for more accurate predictions of their long-term impact. In this study, we used time-lapse imaging to monitor the progression of stem cell colonies in response to various chemical treatments, providing insights into the immediate and long-term effects on pluripotency.

Moreover, high-throughput screening is made feasible through ImageJ's ability to process large datasets quickly and accurately. The automation of image analysis enables the screening of hundreds or even thousands of chemical compounds in parallel. This high-throughput capability is crucial for identifying novel compounds that regulate pluripotency. The integration of ImageJ with automated imaging systems further enhances its utility in large-scale screening efforts, offering an efficient way to identify promising candidates for stem cell-based therapies (Rueden et al 2017; Schindelin et al 2019).

Lastly, the integration and interpretation of data generated by ImageJ with other experimental results, such as gene expression profiling or proteomic analyses, allows for a more holistic understanding of how chemical treatments modulate pluripotency. ImageJ can export data in formats suitable for statistical analysis, enabling researchers to identify significant trends and correlations. This data integration provides a comprehensive view of how individual compounds affect pluripotent stem cells on multiple levels, from morphology to molecular signaling, ultimately supporting the discovery of new therapeutic approaches (Gallagher 2010).

While ImageJ provides an excellent tool for pluripotency screening, there are some limitations to consider. For example, the accuracy of analysis can be influenced by factors such as image quality, sample preparation, and the complexity of biological systems being studied. Future improvements in imaging techniques, including higher-resolution microscopy and advanced fluorescence detection methods, could enhance the capabilities of ImageJ in capturing more subtle cellular changes and improving the reliability of analysis (Hartig 2013).

Additionally, while ImageJ can efficiently quantify morphological changes and marker expression, its ability to analyze more complex biological processes, such as gene regulation, signal transduction, or epigenetic modifications, is limited by its focus on image-based data. To address this, future research could combine ImageJ with other omics technologies, such as RNA sequencing or mass spectrometry, to gain a more comprehensive understanding of how chemical compounds influence pluripotency at the molecular level. The development of more advanced algorithms and machine learning approaches could improve the automation and accuracy of ImageJ's analysis, allowing for even more sophisticated high-throughput screening and data interpretation. These innovations could help bridge the gap between image-based phenotyping

and functional genomics, enabling deeper insights into the molecular networks that control pluripotency and differentiation.

4.2 Optimization of Parameters to Customize ImageJ Analysis

The analyses conducted herein highlight the importance of fine-tuning threshold and particle inclusion size settings to achieve accurate colony detection. Automatic thresholding provides efficiency but often requires manual adjustment to account for variability in image quality, colony characteristics, and experimental conditions. The results presented herein also illustrate the challenges of extreme threshold settings—low thresholds tend to overestimate colony areas by including noise, while high thresholds risk excluding smaller colonies and relevant features. Optimized threshold settings that balance these extremes produce the most reliable results Caverzasio et al 2007).

Particle inclusion size settings also play a pivotal role in colony detection accuracy. Smaller particle sizes are prone to capturing irrelevant debris, leading to false positives, whereas larger sizes risk excluding smaller colonies, underestimating the total colony count. Intermediate particle inclusion sizes, around 20,000 pixels, provided the best balance between specificity and sensitivity, as they excluded noise while retaining valid colonies (Stoddart 2011).

In addition, decisions about hole inclusion can significantly influence detection accuracy. Including holes helps identify hollow colonies—potential indicators of differentiation—while excluding holes simplifies solid colony detection but may lead to misclassification. The relevance of morphological features like hollow centers should guide this decision based on experimental goals (Schindelin et al 2012).

Quantitative analysis using mean gray value, circularity, and area fraction further informed the evaluation of colony characteristics in this study. Lower mean gray values were associated with darker-stained colonies, reflecting higher pluripotency levels. Circularity values provided insights into colony uniformity, with higher values indicating undifferentiated and compact colonies. Area fraction measurements revealed the extent of colony proliferation, offering a metric to compare growth rates across different conditions (Stossi and Singh 2023).

To reduce biases and improve data interpretability, normalized intensity values were calculated by dividing the mean gray value by circularity. This composite metric effectively integrated intensity and shape information, enabling more nuanced comparisons. The approach demonstrates how normalization can enhance the robustness of quantitative analyses in colony detection studies.

Together, these findings emphasize that colony detection parameters cannot be universally standardized due to inherent variability in imaging conditions and colony morphology. Instead, dynamic adjustments tailored to specific experimental setups are necessary to ensure accurate and reproducible results. Researchers must carefully balance detection sensitivity with specificity, considering the impact of these parameters on the accuracy of colony counts and morphological assessments.

4.3 Contrasting Observed Expected Results for Chemical Manipulators

The chemicals tested here were chosen based on differential expression of kinases and receptors identified through prior RNA sequencing and protein microarray studies. Based on the knowledge that aggregation causes cells to differentiate and the fact that cells cultured in the suspension bioreactor with 60 rpm rotation speeds yielded two distinct expression signatures (one associated with naïve pluripotent cells and one associated with differentiation), the chemical

modulators were expected to exert a certain result on pluripotency as outlined in Table 3). While the image analysis was somewhat successful in studying and identifying the effects of the chemicals, it yielded mixed results. For some chemicals, the observed outcomes aligned with the expected results, while for others, discrepancies were noted. This discrepancy may be due to the limits of the image analysis as outlined above but may also stem from the fact that the gene signatures of the cells in the bioreactor stemmed from two different populations. Thus, our results shall be discussed in the context of the knowledge that exists about the chemicals used herein and the pathways that they modulate.

Asiatic Acid, a natural triterpenoid from *Centella asiatica*, activates **p38 MAPK**, a kinase involved in stress responses, inflammation, differentiation, and apoptosis. This activation leads to phosphorylation of downstream targets like **ATF2**, **Elk-1**, and **CHOP**, promoting cellular processes. Activation by Asiatic Acid can increase **PP** by supporting cell differentiation and proliferation, particularly relevant in wound healing and tissue repair. Its ability to modulate p38 MAPK makes it a promising candidate for therapeutic applications in wound healing, tissue regeneration, and conditions requiring controlled proliferation and differentiation, such as fibrotic diseases.

The compound 740 Y-P TFA is a synthetic PI3K activator that plays a critical role in activating the PI3K/Akt signaling pathway, a key regulator of cellular processes like proliferation, survival, and differentiation. It works by increasing the levels of PIP3, which activates downstream signaling proteins such as Akt. In this study, the data confirms 740 Y-P TFA as an effective activator of PI3K, leading to a significant increase in the PP, with a particularly strong impact observed in differentiation processes, as indicated by the green highlight. This underscores the compound's effectiveness in modulating PI3K signaling and its potential for influencing cellular outcomes like differentiation in therapeutic or experiments.

IGF1R Inhibitors BMS-536924 and Linsitinib both reduce PP as expected, with BMS-536924 showing a particularly strong impact (compare green highlight, Table 3). This supports the role of IGF1R in regulating PP and highlights IGF1R inhibition as a viable therapeutic strategy.

Epiblastin A is a selective inhibitor of CK1α, a serine/threonine kinase that plays a crucial role in regulating various cellular processes, including cell cycle control, apoptosis, and signaling pathways like Wnt. CK1α is involved in the regulation of several key processes, particularly those associated with the Wnt signaling pathway, and its inhibition can affect cellular functions such as proliferation, differentiation, and survival. By inhibiting CK1α, Epiblastin A disrupts the regulatory functions of CK1α, which may alter cellular signaling, leading to changes in processes like cell cycle progression, migration, and differentiation. In the present study, CK1α Inhibitor Epiblastin A reduced PP as expected, confirming CK1α's role in regulating PP. The highlight in green in Table 3 suggests the effect aligns with expectations confirming CK1α's potential as a therapeutic target.

LY6 is a SHP2 inhibitor, targeting a tyrosine phosphatase that regulates crucial signaling pathways involved in cell growth, survival, differentiation, and migration, including the RAS/RAF/MEK/ERK, PI3K/AKT, and JAK/STAT pathways. By inhibiting SHP2's phosphatase activity, LY6 blocks the activation of key growth and survival pathways. This inhibition has potential therapeutic applications, particularly in cancer, where it can disrupt oncogenic signaling and limit tumor growth and metastasis, and in autoimmune diseases, where it may reduce immune cell activation and modulate overactive immune responses. Overall, LY6 could decrease cellular proliferation, survival, and migration, making it a promising candidate for treating diseases with dysregulated cellular signaling. Ly6 increased PP in contrast to the expected outcome in our study.

Insulin, through activation of IRS1 (Insulin Receptor Substrate 1), can lead to an increase in PP by mediating key signaling pathways that regulate cell metabolism, growth, and

differentiation. Upon binding to its receptor, insulin activates IRS1, which then triggers downstream cascades, including the PI3K/AKT and MAPK/ERK pathways. These pathways are crucial for promoting cell proliferation, survival, and differentiation. Particularly, the PI3K/AKT pathway regulates cellular growth and metabolism, while the MAPK/ERK pathway influences cell division and differentiation. As a result, insulin's activation of IRS1 enhances PP, promoting cell growth and division in tissues sensitive to insulin signaling, such as adipose tissue, liver, muscle, and cancer cells. This process is vital for maintaining metabolic homeostasis, but in pathological conditions like cancer, dysregulated insulin signaling may contribute to tumor progression. Thus, insulin's role in activating IRS1 is central to both normal cellular function and potential in disease progression. In our study, insulin had no remarkable effect on PP.

The activation of LKB1 by TMPA is likely to reduce PP, as LKB1 activation typically leads to the activation of AMPK, which plays a central role in regulating cellular energy metabolism and maintaining cellular integrity under stress. AMPK activation inhibits the mTOR pathway, a major regulator of cell growth and proliferation. By suppressing mTOR, TMPA's activation of LKB1 may reduce processes related to cell proliferation, leading to a decrease in PP. This is especially relevant in cancer, where enhanced LKB1 or AMPK activity may suppress uncontrolled cell proliferation. Thus, TMPA may decrease PP, contributing to its potential therapeutic value in diseases involving excessive cell proliferation, such as cancer, or in metabolic disorders where cellular homeostasis is disrupted. our results coincide with the earlier research as PP reduces with the increase in the concentration of TMPA.

PDGFRβ activator PDGF-BB increased PP in contrast to the expected outcome, validating PDGFRβ's role in promoting proliferation and differentiation. The absence of highlighting this

result in Table 3 suggests that the results are not particularly novel but confirm PDGFRβ activation's relevance in cellular signaling.

JNK Inhibitor reduced PP as expected, with the green highlight in Table 3 indicating a significant impact. This suggests that the JNK pathway is potentially essential in regulating PP, supporting JNK inhibition as a therapeutic strategy.

EGFR Inhibitor Gefitinib effectively reduced PP, highlighting EGFR's critical role in regulating PP. The green highlight in Table 3 reinforced its potential as a therapeutic target for modulating cell growth and survival.

MP7 is a selective inhibitor of PDK1, a central kinase in the PI3K/Akt signaling pathway, which regulates critical cellular processes like survival, proliferation, metabolism, and growth. MP7 inhibits PDK1, blocking its ability to phosphorylate Akt at Thr308, a key step required for Akt activation. Without this activation, Akt cannot fully transmit its downstream pro-survival and proliferative signals. MP7 reduces the activation of Akt and its downstream signaling by inhibiting PDK1, leading to a decrease in PP. This reflects diminished cellular proliferation and survival signals, making MP7 potentially useful in conditions where inhibition of excessive cell growth is beneficial, such as in cancer treatment. Our results align with expectations, showing a reduction in PP, thereby confirming the critical role of PDK1 and Akt signaling in regulating these cellular functions.

FAK Inhibitors Y15 and YH-306 increase PP, confirming the role of FAK in regulating PP with a yellow highlight (compare Table 3) suggesting that the effect may have additional significance implications. TAK1 activation that triggers downstream signaling pathways, influencing various biological outcomes such as cell proliferation, survival, differentiation, and inflammation. Activation of TAK1 leads to the phosphorylation and activation of key transcription factors like NF-

κB and AP-1, which regulate genes involved in inflammation and cell survival. The activation of TAK1 is expected to increase PP, supporting the role of TAK1 in promoting cellular growth and survival and its potential therapeutic applications in cancer and inflammatory diseases.

This study provides valuable insights into the regulation of PP through different signaling pathways and their potential therapeutic implications. Insulin's role in activating IRS1 to promote PP was confirmed, but no significant effect was observed, suggesting alternative regulatory factors. The activation of AMPK via LKB1 by TMPA effectively reduced PP, supporting its use in therapeutics like cancer. PDGF-BB activation increased PP, reaffirming the role of PDGFRβ in cell proliferation. Reducing PKC activity decreased PP, suggesting PKC inhibition as a therapeutic approach. MP7 inhibition of PDK1 led to reduced PP, emphasizing the importance of the PI3K/Akt pathway in regulating cell growth and survival.

PAK1 is implicated in diseases such as cancer, neurodegenerative disorders, and cardiovascular diseases. G5555 and NVS-PAK-1 inhibit PAK1's kinase activity, preventing its interaction with downstream signaling effectors and disrupting key processes such as cell migration, growth, and survival. In the study, both inhibitors reduced PP, indicating that inhibiting PAK1 can limit aberrant cell proliferation, making these inhibitors promising candidates for treating cancer and diseases linked to PAK1 activation, such as neurodegenerative diseases.

These findings suggest promising therapeutic strategies that target these signaling pathways to regulate cell proliferation, survival, and differentiation in various diseases.

LY215722 can reduce the production of proteins involved in fibrosis, suppress tumor metastasis, and potentially enhance the immune response by inhibiting TGF-β. In terms of cell proliferation and differentiation, LY215722 could decrease PP by inhibiting TGF-β-induced signaling, making it

a promising therapeutic tool for conditions where TGF-β is overactive, such as in cancer, fibrosis, and immune suppression.

G5555 and NVS-PAK1-1 are both PAK1 inhibitors, specifically designed to target PAK1, a key enzyme involved in regulating cellular functions such as migration, proliferation, survival, and cytoskeletal reorganization. PAK1 is implicated in a range of diseases, including cancer, neurodegenerative diseases, and cardiovascular conditions. G5555 is a small molecule inhibitor that blocks PAK1's kinase activity, preventing its interaction with downstream signaling effectors.

5 CONCLUSION

The use of ImageJ in chemical screening of pluripotency presents a robust and efficient approach to analyzing the effects of various compounds on stem cell behavior. By enabling the automated and quantitative analysis of key parameters such as cell morphology, marker expression, proliferation, and viability, ImageJ provides valuable insights into the molecular mechanisms that regulate pluripotency. The ability to track dynamic changes in cell morphology and marker expression in real-time further enhances our understanding of the impact of chemical treatments on stem cell fate.

This study demonstrates that ImageJ is not only an effective tool for high-throughput screening, but also an essential resource for identifying compounds that modulate pluripotency. Its capacity to process fluorescence images and analyze time-lapse data facilitates the detection of subtle changes in stem cell behavior, providing a comprehensive platform for pluripotency screening.

Moreover, the integration of ImageJ with other experimental techniques, such as gene expression profiling and proteomics, can offer a deeper understanding of the signaling pathways and molecular networks governing stem cell self-renewal and differentiation. This approach can

expedite the discovery of novel compounds for stem cell-based therapies and regenerative medicine applications, supporting the development of more efficient and targeted treatments.

Overall, ImageJ serves as a powerful tool for advancing our knowledge of pluripotency regulation, making it a crucial asset in the field of stem cell research and therapeutic development. Future research can enhance the use of ImageJ by combining it with omics technologies to better understand the complex mechanisms regulating stem cell fate. As imaging and computational tools advance, ImageJ will provide deeper insights into pluripotency regulation and support the discovery of new therapeutic strategies for regenerative medicine. The analysis highlights the importance of fine-tuning threshold and particle inclusion size settings to achieve accurate colony detection. Automatic thresholding provides efficiency but often requires manual adjustment to account for variability in image quality, colony characteristics, and experimental conditions. Figures 10 and 11 illustrate the challenges of extreme threshold settings—low thresholds tend to overestimate colony areas by including noise, while high thresholds risk excluding smaller colonies and relevant features. Optimized threshold settings that balance these extremes produce the most reliable results.

Particle inclusion size settings also play a pivotal role in colony detection accuracy. Smaller particle sizes are prone to capturing irrelevant debris, leading to false positives, whereas larger sizes risk excluding smaller colonies, underestimating the total colony count. Intermediate particle inclusion sizes, around 20,000 pixels, provided the best balance between specificity and sensitivity, as they excluded noise while retaining valid colonies.

In addition, decisions about hole inclusion can significantly influence detection accuracy. Including holes helps identify hollow colonies as potential indicators of differentiation while excluding holes simplifies solid colony detection but may lead to misclassification. The relevance

of morphological features like hollow centers should guide this decision based on experimental goals.

Quantitative analysis using mean gray value, circularity, and area fraction further informed the evaluation of colony characteristics. Lower mean gray values were associated with darker-stained colonies, reflecting higher pluripotency levels. Circularity values provided insights into colony uniformity, with higher values indicating undifferentiated and compact colonies. Area fraction measurements revealed the extent of colony proliferation, offering a metric to compare growth rates across different conditions.

To reduce biases and improve data interpretability, normalized intensity values were calculated by dividing the mean gray value by circularity. This composite metric effectively integrated intensity and shape information, enabling more nuanced comparisons. The approach demonstrates how normalization can enhance the robustness of quantitative analyses in colony detection studies.

The findings emphasize that colony detection parameters cannot be universally standardized due to inherent variability in imaging conditions and colony morphology. Instead, dynamic adjustments tailored to specific experimental setups are necessary to ensure accurate and reproducible results. Researchers must carefully balance detection sensitivity with specificity, considering the impact of these parameters on the accuracy of colony counts and morphological assessments.

The present study provides a systematic approach to optimizing colony detection in image analysis. A combination of tailored thresholding, intermediate particle inclusion sizes, and careful consideration of hole inclusion can significantly improve accuracy. These findings are valuable for researchers aiming to enhance reproducibility and precision in colony detection workflows.

6 FUTURE WORK

The image analysis has identified potential chemical combinations that may be effective in maintaining pluripotency. The next phase of research will involve exposing human embryonic stem cells to these chemical combinations over ten passages to further investigate their effects on pluripotency.

Following this, a pluripotency dot blot, designed to detect specific proteins associated with pluripotency, will be performed to confirm the maintenance of pluripotent markers. This technique, likely a form of Differential Immunoblotting (DIT), will assess the expression levels of key pluripotency markers in the treated stem cells.

Subsequently, a teratoma formation assay will be conducted. This test involves the injection of pluripotent stem cells into immunocompromised animals (e.g., mice or rats) to observe whether the injected cells form a teratoma—a tumor composed of differentiated tissues from all three primary germ layers (ectoderm, mesoderm, and endoderm). The successful formation of a teratoma would confirm the pluripotency of the stem cells, demonstrating their ability to differentiate into cell types from all three germ layers.

Finally, after validating the chemical combinations through these assays, the chemicals will be tested in a bioreactor environment to assess their efficacy in maintaining pluripotency under more complex, dynamic conditions.

7 REFERENCES

1. Ahsan, T. A.M. Doyle, R.M. Nerem,3 - Stem Cell Research,Editor(s): Anthony Atala, Robert Lanza, James A. Thomson, Robert M. Nerem,Principles of Regenerative Medicine,AcademicPress,2008,28-47,ISBN9780123694102.

2. Apáti, A., Varga, N., Berecz, T., Erdei, Z., Homolya, L., & Sarkadi, B. (2018). Application of human pluripotent stem cells and pluripotent stem cell-derived cellular models for assessing drug toxicity. *Expert Opinion on Drug Metabolism & Toxicology*, *15*(1), 61–75.

3. Appiah-Kubi, K. Y. Wang, H. Qian, M. Wu, X. Yao, Y. Wu, Y. Chen Platelet-derived growth factor receptor/platelet-derived growth factor (PDGFR/PDGF) system is a prognostic and treatment response biomarker with multifarious therapeutic targets in cancers Tumor Biol., 37 (8) (2016), pp. 10053-10066

4. Armstrong L., Hughes O., Yung S., Hyslop L., Stewart R., Wappler I., Peters H., Walter T., Stojkovic P., Evans J., et al. The role of PI3K/AKT, MAPK/ERK and NFκβ signalling in the maintenance of human embryonic stem cell pluripotency and viability highlighted by transcriptional profiling and functional analysis. Hum. Mol. Genet. 2006;15:1894–1913

5. Audronė V. Kalvelytė, Aušra Imbrasaitė, Natalija Krestnikova, Aurimas Stulpinas,Chapter Four - Adult Stem Cells and Anticancer Therapy,Editor(s): James C. Fishbein, Jacqueline M. Heilman,Advances in Molecular Toxicology,Elsevier,Volume 11,2017,Pages 123-202,ISSN 1872-0854,ISBN 9780128125229

6. Balbina García-Reyes, Lydia Witt, Björn Jansen, Ebru Karasu, Tanja Gehring, Johann Leban, Doris Henne-Bruns, Christian Pichlo, Elena Brunstein, Ulrich Baumann, Fabian Wesseler, Bernd Rathmer, Dennis Schade, Christian Peifer, and Uwe Knippschild, Discovery of Inhibitor of Wnt Production 2 (IWP-2) and Related Compounds As Selective ATP-Competitive Inhibitors of Casein Kinase 1 (CK1) δ/ε *Journal of Medicinal Chemistry* 2018 *61* (9), 4087-4102

7. Ben-David, U., Gan, Q. F., Golan-Lev, T., Arora, P., Yanuka, O., Oren, Y. S., Leikin-Frenkel, A., Graf, M., Garippa, R., Boehringer, M., Gromo, G., & Benvenisty, N. (2013). Selective elimination of human pluripotent stem cells by an oleate synthesis inhibitor discovered in a high-throughput screen. *Cell stem cell*, *12*(2), 167–179.

8. Blauwkamp, T. A., Nigam, S., Ardehali, R., Weissman, I. L., & Nusse, R. (2012). Endogenous Wnt signalling in human embryonic stem cells generates an equilibrium of distinct lineage-specified progenitors. *Nature communications*, *3*, 1070. https://doi.org/10.1038/ncomms2064

9. Boiani, M., H.R. Schöler. Regulatory networks in embryo-derived pluripotent stem cells Nat. Rev. Mol. Cell Biol, 6 (2005), pp. 872-884

10. Bolte, S., & Cordelières, F. P. (2006). A guided tour into subcellular colocalization analysis in light microscopy. Journal of microscopy, 224(Pt 3), 213–232. https://doi.org/10.1111/j.1365-2818.2006.01706.x

11. Boyer, L.A. T.I. Lee, M.F. Cole, S.E. Johnstone, S.S. Levine, J.P. Zucker, M.G. Guenther, R.M. Kumar, H.L. Murray, R.G. Jenner, D.K. Gifford, D.A. Melton, R. Jaenisch, R.A. Young Core transcriptional regulatory circuitry in human embryonic stem cellsCell, 122 (2005), pp. 947-956

12. Brons IG, Smithers LE, Trotter MW, Rugg-Gunn P, Sun B, Chuva de Sousa Lopes SM, Howlett SK, Clarkson A, Ahrlund-Richter L, Pedersen RA, Vallier L. Derivation of pluripotent epiblast stem cells from mammalian embryos. Nature. 2007 Jul 12;448(7150):191-5. doi: 10.1038/nature05950. Epub 2007 Jun 27. PMID: 17597762.

13. Burdon T, Chambers I, Nichols J, Smith A. Suppression of SHP-2 and ERK signalling promotes self-renewal of mouse embryonic stem cells. *Dev Biol* 1999; 210:30–43.

14. Cantley LC. The phosphoinositide 3-kinase pathway. *Science* 296:1655-1657, 2002

15. Carling, D., Sanders, M. J., & Woods, A. (2008). The regulation of AMP-activated protein kinase by upstream kinases. *International journal of obesity (2005)*, *32 Suppl 4*, S55–S59.

16. Caverzasio J, Manen D. Essential role of Wnt3a-mediated activation of mitogen-activated protein kinase p38 for the stimulation of alkaline phosphatase activity and matrix mineralization in C3H10T1/2 mesenchymal cells. Endocrinology. 2007 Nov;148(11):5323-30. doi: 10.1210/en.2007-0520. Epub 2007 Aug 23. PMID: 17717053.

17. Cerneckis, J., Cai, H. & Shi, Y. Induced pluripotent stem cells (iPSCs): molecular mechanisms of induction and applications. *Sig Transduct Target Ther* 9, 112 (2024). https://doi.org/10.1038/s41392-024-01809-0

18. Chambers I, Colby D, Robertson M, Nichols J, Lee S, Tweedie S, Smith A. Functional expression cloning of Nanog, a pluripotency sustaining factor in embryonic stem cells. Cell. 2003 May 30;113(5):643-55. doi: 10.1016/s0092-8674(03)00392-1. PMID: 12787505.

19. Chen G, Gulbranson DR, Hou Z, Bolin JM, Ruotti V, Probasco MD, Smuga-Otto K, Howden SE, Diol NR, Propson NE, Wagner R, Lee GO, Antosiewicz-Bourget J, Teng JM, Thomson JA. Chemically defined conditions for human iPSC derivation and culture. Nat Methods. 2011 May;8(5):424-9. doi: 10.1038/nmeth.1593. Epub 2011 Apr 10. PMID: 21478862; PMCID: PMC3084903.

20. Chen, K. G., Mallon, B. S., McKay, R. D. G., and Robey, P. G. (2014). Human pluripotent stem cell culture: considerations for maintenance, expansion, and therapeutics. *Cell Stem Cell* 14, 13–26. doi: 10.1016/j.stem.2013.12.005

21. Cheng F, Li M, Thorne RF, Liu G, Zhang Y, Wu M, Liu L. P21-Activated Kinase 4 Pak4 Maintains Embryonic Stem Cell Pluripotency via Akt Activation. Stem Cells. 2022 Oct 21;40(10):892-905. doi: 10.1093/stmcls/sxac050. PMID: 35896382; PMCID: PMC9585903.

22. Cheng, H.D. X.H. Jiang, Y. Sun, Jingli Wang,Color image segmentation: advances and prospects,Pattern Recognition,Volume 34, Issue 12,2001,2259-2281,https://doi.org/10.1016/S0031-3203(00)00149-7

23. Chou YF, Chen HH, Eijpe M, Yabuuchi A, Chenoweth JG, Tesar P, Lu J, McKay RD, Geijsen N. The growth factor environment defines distinct pluripotent ground states in novel blastocyst-derived stem cells. Cell. 2008 Oct 31;135(3):449-61. doi: 10.1016/j.cell.2008.08.035. PMID: 18984157; PMCID: PMC2767270

24. Clevers H. Wnt/beta-catenin signaling in development and disease. Cell. 2006 Nov 3;127(3):469-80. doi: 10.1016/j.cell.2006.10.018. PMID: 17081971.

25. Collins TJ. ImageJ for microscopy. Biotechniques. 2007 Jul;43(1 Suppl):25-30. doi: 10.2144/000112517. PMID: 17936939

26. Conesa, C., Doss, M. X., Antzelevitch, C., Sachinidis, A., Sancho, J., & Carrodeguas, J. A. (2012). Identification of specific pluripotent stem cell death--inducing small molecules by chemical screening. *Stem cell reviews and reports*, *8*(1), 116–127. https://doi.org/10.1007/s12015-011-9248-4

27. Cox N et al. 2021 Diet-regulated production of PDGFcc by macrophages controls energy storage. *Science (New York, NY)* 373, eabe9383

28. Cuadrado A. & Nebreda A. R. Mechanisms and functions of p38 MAPK signalling. The Biochemical journal 429, 403–417, doi: 10.1042/BJ20100323 (2010).

29. Cuenda, A., & Sanz-Ezquerro, J. J. (2017). p38γ and p38δ: From Spectators to Key Physiological Players. *Trends in biochemical sciences*, *42*(6), 431–442. https://doi.org/10.1016/j.tibs.2017.02.008

30. Dalton S. (2013). Signaling networks in human pluripotent stem cells. *Current opinion in cell biology*, *25*(2), 241–246.

31. Danovi, D., Falk, A., Humphreys, P., Vickers, R., Tinsley, J., Smith, A. G., & Pollard, S. M. (2010). Imaging-based chemical screens using normal and glioma-derived neural stem cells. *Biochemical Society transactions*, *38*(4), 1067–1071.

32. Davidson, K. C., Adams, A. M., Goodson, J. M., McDonald, C. E., Potter, J. C., Berndt, J. D., Biechele, T. L., Taylor, R. J., & Moon, R. T. (2012). Wnt/β-catenin signaling promotes differentiation, not self-renewal, of human embryonic stem cells and is repressed by

Oct4. *Proceedings of the National Academy of Sciences of the United States of America*, *109*(12), 4485–4490.

33. Deschamps JP, Nelson B. TGFbeta/activin/nodal signaling is necessary for the maintenance of pluripotency in human embryonic stem cells. Development. 2005;132:1273–1282. doi: 10.1242/dev.01706.

34. Dvorak, P., Dvorakova, D., and Hampl, A. (2006). Fibroblast growth factor signaling in embryonic and cancer stem cells. *FEBS Lett.* 580, 2869–2874. doi: 10.1016/j.febslet.2006.01.095

35. Embryonic stem cell lines derived from human blastocystsScience, 282 (1998), pp. 1145-1147,

36. Feng, GS. Shp2-mediated molecular signaling in control of embryonic stem cell self-renewal and differentiation. *Cell Res* 17, 37–41 (2007).

37. G. Martello, A. SmithThe nature of embryonic stem cells. Annu. Rev. Cell Dev. Biol., 30 (2014), pp. 647-675

38. Gallagher, S.R. (2010), Digital Image Processing and Analysis with ImageJ. Current Protocols Essential Laboratory Techniques, 3: A.3C.1-A.3C.24. https://doi.org/10.1002/9780470089941.eta03cs03

39. Gan B, Hu J, Jiang S, Liu Y, Sahin E, Zhuang L, Fletcher-Sananikone E, Colla S, Wang YA, Chin L, Depinho RA. Lkb1 regulates quiescence and metabolic homeostasis of haematopoietic stem cells. Nature. 2010 Dec 2;468(7324):701-4. doi: 10.1038/nature09595. PMID: 21124456; PMCID: PMC3058342.

40. Gonzalez, R. C., & Woods, R. E. (2017). *Digital Image Processing (4th ed.). Pearson

41. Gross, S. D., & Anderson, R. A. (1998). Casein kinase I: spatial organization and positioning of a multifunctional protein kinase family. *Cellular signalling*, *10*(10), 699–711.

42. Guan, J., Wang, G., Wang, J., Zhang, Z., Fu, Y., Cheng, L., Meng, G., Lyu, Y., Zhu, J., Li, Y., Wang, Y., Liuyang, S., Liu, B., Yang, Z., He, H., Zhong, X., Chen, Q., Zhang, X., Sun, S., Lai, W., … Deng, H. (2022). Chemical reprogramming of human somatic cells to pluripotent stem cells. *Nature*, *605*(7909), 325–331.

43. Gui T, Sun Y, Shimokado A, Muragaki Y. The roles of mitogen-activated protein kinase pathways in TGF-beta-induced epithelial-mesenchymal transition. J Signal Transduct. 2012;2012:289243.

44. Gupta MK, De Jesus DF, Kahraman S, et al. Insulin receptor-mediated signaling regulates pluripotency markers and lineage differentiation. Molecular Metabolism. 2018

Dec;18:153-163. DOI: 10.1016/j.molmet.2018.09.003. PMID: 30316806; PMCID: PMC6308035.

45. Hackett, J. A., & Surani, M. A. (2014). Regulatory principles of pluripotency: from the ground state up. *Cell stem cell*, *15*(4), 416–430. https://doi.org/10.1016/j.stem.2014.09.015

46. Han J, Wu J, Silke J. An overview of mammalian p38 mitogen-activated protein kinases, central regulators of cell stress and receptor signaling. F1000Res. 2020 Jun 29;9:F1000 Faculty Rev-653. doi: 10.12688/f1000research.22092.1. PMID: 32612808; PMCID: PMC7324945.

47. Hartig SM. Basic image analysis and manipulation in ImageJ. Curr Protoc Mol Biol. 2013;Chapter 14:Unit14.15. doi: 10.1002/0471142727.mb1415s102. PMID: 23547012.

48. Hirata, N., Nakagawa, M., Fujibayashi, Y., Yamauchi, K., Murata, A., Minami, I., Tomioka, M., Kondo, T., Kuo, T. F., Endo, H., Inoue, H., Sato, S. I., Ando, S., Kawazoe, Y., Aiba, K., Nagata, K., Kawase, E., Chang, Y. T., Suemori, H., Eto, K., … Uesugi, M. (2014). A chemical probe that labels human pluripotent stem cells. *Cell reports*, *6*(6), 1165–1174

49. Hou, P., Li, Y., Zhang, X., Liu, C., Guan, J., Li, H., Zhao, T., Ye, J., Yang, W., Liu, K., Ge, J., Xu, J., Zhang, Q., Zhao, Y., & Deng, H. (2013). Pluripotent stem cells induced from mouse somatic cells by small-molecule compounds. *Science (New York, N.Y.)*, *341*(6146), 651–654.

50. Huang, J., Guo, X., Li, W. *et al.* Activation of Wnt/β-catenin signalling *via* GSK3 inhibitors direct differentiation of human adipose stem cells into functional hepatocytes. *Sci Rep* 7, 40716 (2017). https://doi.org/10.1038/srep40716

51. Huangfu, D., Maehr, R., Guo, W., Eijkelenboom, A., Snitow, M., Chen, A. E., & Melton, D. A. (2008). Induction of pluripotent stem cells by defined factors is greatly improved by small-molecule compounds. *Nature biotechnology*, *26*(7), 795–797. https://doi.org/10.1038/nbt1418

52. J. Sei, B. Moses, A. Harris Becker, M. Kim, N. Kaur, M. Vemuri, C. Civin,StemPro™ HSC expansion medium (Prototype) supports superior expansion of human hematopoietic stem-progenitor cells,Cytotherapy, Volume 21, Issue 5, Supplement,2019,S64-S65,

53. J. Liu, S. Pan, M.H. Hsieh, N. Ng, F. Sun, T. Wang, S. Kasibhatla, A.G. Schuller, A.G. Li, D. Cheng, J. Li, C. Tompkins, A. Pferdekamper, A. Steffy, J. Cheng, C. Kowal, V. Phung, G. Guo, Y. Wang, M.P. Graham, S. Flynn, J.C. Brenner, C. Li, M.C. Villarroel, P.G. Schultz, X. Wu, P. McNamara, W.R. Sellers, L. Petruzzelli, A.L. Boral, H.M. Seidel, M.E. McLaughlin, J. Che, T.E. Carey, G. Vanasse, J.L. Harris, Targeting Wnt-driven cancer through the inhibition of Porcupine by LGK974, *Proc. Natl. Acad. Sci. U.S.A.* 110 (50) 20224-20229 (2013).

54. J.A. Thomson, J. Itskovitz-
Eldor, S.S. Shapiro, M.A. Waknitz, J.J. Swiergiel, V.S. Marshall, J.M. Jones

55. James D, Levine AJ, Besser D, Hemmati-Brivanlou A. TGFbeta/activin/nodal signaling is necessary for the maintenance of pluripotency in human embryonic stem cells. Development. 2005;132:1273–1282. doi: 10.1242/dev.01706.

56. Jensen, E.C. (2013), Quantitative Analysis of Histological Staining and Fluorescence Using ImageJ. Anat. Rec., 296: 378-381. https://doi.org/10.1002/ar.22641

57. Jiang S, Zhang M, Sun J, Yang X. Casein kinase 1α: biological mechanisms and theranostic potential. Cell Commun Signal. 2018 May 24;16(1):23. doi: 10.1186/s12964-018-0236-z. PMID: 29793495; PMCID: PMC5968562.

58. Kahn-Krell Asher, Pretorius Danielle , Ou Jianfa , Fast Vladimir G. , Litovsky Silvio , Berry Joel , Liu Xiaoguang (Margaret) , Zhang Jianyi .Bioreactor Suspension Culture: Differentiation and Production of Cardiomyocyte Spheroids From Human Induced Pluripotent Stem Cells.Frontiers in Bioengineering and Biotechnology 9 2021https://www.frontiersin.org/journals/bioengineering-and biotechnology/articles/10.3389/fbioe.2021.674260 DOI=10.3389/fbioe.2021.674260

59. Katarzyna Marzec-Schmidt, Nidal Ghosheh, Sören Richard Stahlschmidt, Barbara Küppers-Munther, Jane Synnergren, Benjamin Ulfenborg, Artificial Intelligence Supports Automated Characterization of Differentiated Human Pluripotent Stem Cells, *Stem Cells*, Volume 41, Issue 9, September 2023, Pages 850–861, https://doi.org/10.1093/stmcls/sxad049

60. Kehoe DE, Jing D, Lock LT, Tzanakakis ES. Scalable stirred-suspension bioreactor culture of human pluripotent stem cells. Tissue Eng Part A. 2010 Feb;16(2):405-21. doi: 10.1089/ten.tea.2009.0454. PMID: 19739936; PMCID: PMC2813185.

61. Keller, G. (2005). Embryonic stem cell differentiation: emergence of a new era in biology and medicine. *Genes and Development, 19*, 1129–1155.

62. Kim H, Kim S, Song Y, Kim W, Ying QL, Jho EH. Dual Function of Wnt Signaling during Neuronal Differentiation of Mouse Embryonic Stem Cells. Stem Cells Int. 2015;2015:459301. doi: 10.1155/2015/459301. Epub 2015 Apr 5. PMID: 25945099; PMCID: PMC4402205.

63. Kim, J. Y., Nam, Y., Rim, Y. A., & Ju, J. H. (2022). Review of the Current Trends in Clinical Trials Involving Induced Pluripotent Stem Cells. *Stem cell reviews and reports*, *18*(1), 142–154. https://doi.org/10.1007/s12015-021-10262-3

64. Kim, Y., Jeong, J. Choi, D. Small-molecule-mediated reprogramming: a silver lining for regenerative medicine. *Exp Mol Med* **52**, 213–226 (2020). https://doi.org/10.1038/s12276-020-0383-3

65. Komal Loya,Chapter 11 - Stem Cells,Editor(s): Sandosh Padmanabhan,Handbook of Pharmacogenomics and Stratified Medicine,Academic Press,2014,Pages 207-231,ISBN 9780123868824,https://doi.org/10.1016/B978-0-12-386882-4.00011-6

66. Krawetz, R., Taiani, J. T., Liu, S., Meng, G., Li, X., Kallos, M. S., & Rancourt, D. E. (2010). Large-scale expansion of pluripotent human embryonic stem cells in stirred-suspension bioreactors. *Tissue engineering. Part C, Methods*, *16*(4), 573–582

67. Kudaravalli, S., den Hollander, P. & Mani, S.A. Role of p38 MAP kinase in cancer stem cells and metastasis. *Oncogene* 41, 3177–3185 (2022).

68. Kusserow A, Pang K, Sturm C, Hrouda M, Lentfer J, Schmidt HA, Technau U, von Haeseler A, Hobmayer B, Martindale MQ, Holstein TW. Unexpected complexity of the Wnt gene family in a sea anemone. Nature. 2005 Jan 13;433(7022):156-60. doi: 10.1038/nature03158. PMID: 15650739.

69. Labusca, L., & Mashayekhi, K. (2019). Human adult pluripotency: Facts and questions. *World journal of stem cells*, *11*(1), 1–12.

70. Lange, L., Esteban, M. A., & Schambach, A. (2022). Back to pluripotency: fully chemically induced reboot of human somatic cells. *Signal transduction and targeted therapy*, *7*(1), 244.

71. Lannon, C., Moody, J., King, D. *et al.* A defined, feeder-independent medium for human embryonic stem cell culture. *Cell Res* 18 (Suppl 1), S34 (2008). https://doi.org/10.1038/cr.2008.124

72. Levine AJ, Puzio-Kuter AM, Chan CS, Hainaut P. The Role of the p53 Protein in Stem-Cell Biology and Epigenetic Regulation. Cold Spring Harb Perspect Med. 2016 Sep 1;6(9):a026153. doi: 10.1101/cshperspect.a026153. PMID: 27352800; PMCID: PMC5008064.

73. Li Q.V., Dixon G., Verma N., Rosen B.P., Gordillo M., Luo R., Xu C., Wang Q., Soh C.-L., Yang D., et al. Genome-scale screens identify JNK–JUN signaling as a barrier for pluripotency exit and endoderm differentiation. Nat. Genet. 2019;51:999–1010. doi: 10.1038/s41588-019-0408-9.

74. Li X, Kaur N, Albahrani M, Karpf AR, Black AR, Black JD. Crosstalk between protein kinase C α and transforming growth factor β signaling mediated by Runx2 in intestinal epithelial cells. J Biol Chem. 2023 Apr;299(4):103017. doi: 10.1016/j.jbc.2023.103017. Epub 2023 Feb 13. PMID: 36791912; PMCID: PMC10036670

75. Li Z. & Rana T. M. A. MEK/ERK signaling contributes to the maintenance of human embryonic stem cell self-renewal. Differentiation; research in biological diversity 75, 299–307, doi: 10.1111/j.1432-0436.2006.00143.x (2007)

76. Li, S., Li, M., Liu, X., Yang, Y., Wei, Y., Chen, Y., Qiu, Y., Zhou, T., Feng, Z., Ma, D., Fang, J., Ying, H., Wang, H., Musunuru, K., Shao, Z., Zhao, Y., & Ding, Q. (2018). Genetic and Chemical Screenings Identify HDAC3 as a Key Regulator in Hepatic Differentiation of Human Pluripotent Stem Cells. *Stem cell reports*, *11*(1), 22–31.

77. Liu, C., Li, Y., Semenov, M., Han, C., Baeg, G. H., Tan, Y., Zhang, Z., Lin, X., & He, X. (2002). Control of beta-catenin phosphorylation/degradation by a dual-kinase mechanism. *Cell*, *108*(6), 837–847. https://doi.org/10.1016/s0092-8674(02)00685-2

78. Liu, J., Xiao, Q., Xiao, J. *et al.* Wnt/β-catenin signalling: function, biological mechanisms, and therapeutic opportunities. *Sig Transduct Target Ther* 7, 3 (2022). https://doi.org/10.1038/s41392-021-00762-6

79. Liu, J., Xiao, Q., Xiao, J. *et al.* Wnt/β-catenin signalling: function, biological mechanisms, and therapeutic opportunities. *Sig Transduct Target Ther* 7, 3 (2022). https://doi.org/10.1038/s41392-021-00762-6

80. Liuyang, S., Wang, G., Wang, Y., He, H., Lyu, Y., Cheng, L., Yang, Z., Guan, J., Fu, Y., Zhu, J., Zhong, X., Sun, S., Li, C., Wang, J., & Deng, H. (2023). Highly efficient and rapid generation of human pluripotent stem cells by chemical reprogramming. *Cell stem cell*, *30*(4), 450–459.e9. https://doi.org/10.1016/j.stem.2023.02.008

81. Long Y, Wang M, Gu, H., & Xie, X. (2015). Bromodeoxyuridine promotes full-chemical induction of mouse pluripotent stem cells. *Cell research*, *25*(10), 1171–1174. https://doi.org/10.1038/cr.2015.96

82. Lyssiotis, C. A., Foreman, R. K., Staerk, J., Garcia, M., Mathur, D., Markoulaki, S., Hanna, J., Lairson, L. L., Charette, B. D., Bouchez, L. C., Bollong, M., Kunick, C., Brinker, A., Cho, C. Y., Schultz, P. G., & Jaenisch, R. (2009). Reprogramming of murine fibroblasts to induced pluripotent stem cells with chemical complementation of Klf4. *Proceedings of the National Academy of Sciences of the United States of America*, *106*(22), 8912–8917

83. Madrid JV, Vera-Colón MKM, Zur Nieden NI. Perturbations in Osteogenic Cell Fate Following Exposure to Constituents Present in Tobacco: A Combinatorial Study. Toxics. 2023 Dec 7;11(12):998. doi: 10.3390/toxics11120998. PMID: 38133399; PMCID: PMC10747453.

84. Madsen, R. R. (2019). *Investigation of genetic PIK3CA activation in genome-edited human pluripotent stem cells*.

85. Marianne E. Yassa, Iman A. Mansour, Nadia I. Sewelam, Hala Hamza, Taghrid Gaafar,The impact of growth factors on human induced pluripotent stem cells differentiation into cardiomyocytes, Life Sciences, Volume 196,2018,8-47,https://doi.org/10.1016/j.lfs.2018.01.009

86. Masayo Sakaki-Yumoto, Jianming Liu, Miguel Ramalho-Santos, Nobuaki Yoshida, Rik Derynck,Smad2 Is Essential for Maintenance of the Human and Mouse Primed

Pluripotent Stem Cell State,Journal of Biological Chemistry,Volume 288, Issue 25,2013, 18546-18560,

87. Massagué J., Seoane J., Wotton D. Smad transcription factors. Genes Dev. 2005;19:2783–2810. doi: 10.1101/gad.1350705.

88. McLaren, D., Gorba, T., Marguerie de Rotrou, A., Pillai, G., Chappell, C., Stacey, A., Lingard, S., Falk, A., Smith, A., Koch, P., Brüstle, O., Vickers, R., Tinsley, J., Flanders, D., Bello, P., & Craig, S. (2013). Automated large-scale culture and medium-throughput chemical screen for modulators of proliferation and viability of human induced pluripotent stem cell-derived neuroepithelial-like stem cells. *Journal of biomolecular screening*, *18*(3), 258–268

89. McLean A.B., D'Amour K.A., Jones K.L., Krishnamoorthy M., Kulik M.J., Reynolds D.M., Sheppard A.M., Liu H., Xu Y., Baetge E.E., et al. Activin a efficiently specifies definitive endoderm from human embryonic stem cells only whenphosphatidylinositol 3-kinase signaling is suppressed. Stem Cells. 2007;25:29–38. doi: 10.1634/stemcells.2006-0219.

90. Mossahebi-Mohammadi M, Quan M, Zhang JS, Li X. FGF Signaling Pathway: A Key Regulator of Stem Cell Pluripotency. Front Cell Dev Biol. 2020 Feb 18;8:79. doi: 10.3389/fcell.2020.00079. PMID: 32133359; PMCID: PMC7040165.

91. N. Otsu, "A Threshold Selection Method from Gray-Level Histograms," in *IEEE Transactions on Systems, Man, and Cybernetics*, vol. 9, no. 1, pp. 62-66, Jan. 1979, doi: 10.1109/TSMC.1979.4310076.

92. N. Otsu, A Threshold Selection Method from Gray-Level Histograms, in *IEEE Transactions on Systems, Man, and Cybernetics*, vol. 9, no. 1, pp. 62-66, Jan. 1979, doi: 10.1109/TSMC.1979.4310076

93. Nagasaka R, Matsumoto M, Okada M, Sasaki H, Kanie K, Kii H, Uozumi T, Kiyota Y, Honda H, Kato R. Visualization of morphological categories of colonies for monitoring of effect on induced pluripotent stem cell culture status. Regen Ther. 2017 Feb 10;6:41-51. doi: 10.1016/j.reth.2016.12.003. PMID: 30271838; PMCID: PMC6134894.

94. National Research Council (US) and Institute of Medicine (US) Committee on the Biological and Biomedical Applications of Stem Cell Research. Stem Cells and the Future of Regenerative Medicine. Washington (DC): National Academies Press (US); 2002. CHAPTER TWO, Adult Stem Cells. Available from: https://www.ncbi.nlm.nih.gov/books/NBK223693/

95. Neganova I, Chichagova V, Armstrong L, Lako M. A critical role for p38MAPK signalling pathway during reprogramming of human fibroblasts to iPSCs. Sci Rep. 2017 Feb 3;7:41693. doi: 10.1038/srep41693. PMID: 28155868; PMCID: PMC5290526.

96. Newton AC (1997) Regulation of protein kinase C. Curr. Opin. Cell Biol. 9: 161–167.

97. Nusse R, Varmus HE. Many tumors induced by the mouse mammary tumor virus contain a provirus integrated in the same region of the host genome. Cell. 1982 Nov;31(1):99-109. doi: 10.1016/0092-8674(82)90409-3. PMID: 6297757.

98. Nusse, R., & Clevers, H. (2017). Wnt/β-Catenin Signaling, Disease, and Emerging Therapeutic Modalities. *Cell*, *169*(6), 985–999.

99. Paling, N. R., Wheadon, H., Bone, H. K., & Welham, M. J. (2004). Regulation of embryonic stem cell self-renewal by phosphoinositide 3-kinase-dependent signaling. *The Journal of biological chemistry*, *279*(46), 48063–48070.

100. Papanayotou C, Collignon J. Activin/Nodal signalling before implantation: setting the stage for embryo patterning. Philos Trans R Soc Lond B Biol Sci. 2014 Dec 5;369(1657):20130539. doi: 10.1098/rstb.2013.0539. PMID: 25349448; PMCID: PMC4216462.

101. Pratibha Pandey, Fahad Khan, Tarun Kumar Upadhyay, Moon Seungjoon, Moon Nyeo Park, Bonglee Kim,New insights about the PDGF/PDGFR signaling pathway as a promising target to develop cancer therapeutic strategies,Biomedicine & Pharmacotherapy,Volume 161,2023,114491,

102. Proffitt KD, Virshup DM. Precise regulation of porcupine activity is required for physiological Wnt signaling. J Biol Chem. 2012 Oct 5;287(41):34167-78.doi: 10.1074/jbc.M112.381970 .

103. Qi X, Li TG, Hao J, Hu J, Wang J, Simmons H, Miura S, Mishina Y, Zhao GQ. BMP4 supports self-renewal of embryonic stem cells by inhibiting mitogen-activated protein kinase pathways. Proc Natl Acad Sci U S A. 2004 Apr 20;101(16):6027-32. doi: 10.1073/pnas.0401367101. Epub 2004 Apr 9. PMID: 15075392; PMCID: PMC395917.

104. Qian Y, Chen X. Senescence regulation by the p53 protein family. Methods Mol Biol. 2013;965:37-61. doi: 10.1007/978-1-62703-239-1_3. PMID: 23296650; PMCID: PMC3784259.

105. Rafael C. Gonzalez, Richard E. Woods. Digital Image Processing.Second Edition. Prentice Hall 2002

106. Ralitsa R. Madsen, James Longden, Rachel G. Knox, Xavier Robin, Franziska Völlmy, Kenneth G. Macleod, Larissa S. Moniz, Neil O. Carragher, Rune Linding, Bart Vanhaesebroeck, Robert K. Semple; NODAL/TGFβ signalling mediates the self-sustained stemness induced by *PIK3CA*^{H1047R} homozygosity in pluripotent stem cells. *Dis Model Mech* 1 March 2021; 14 (3): dmm048298.

107. Ralph Graichen, Xiuqin Xu, Stefan R. Braam, Thavamalar Balakrishnan, Siti Norfiza, Shirly Sieh, Set Yen Soo, Su Chin Tham, Christine Mummery, Alan Colman, Robert Zweigerdt, Bruce P. Davidson Enhanced cardiomyogenesis of human embryonic stem cells by a

small molecular inhibitor of p38 MAPK, Differentiation,Volume 76, Issue 4,2008,Pages 357-370,

108. Ramazzotti G, Ratti S, Fiume R, Follo MY, Billi AM, Rusciano I, Owusu Obeng E, Manzoli L, Cocco L, Faenza I. Phosphoinositide 3 Kinase Signaling in Human Stem Cells from Reprogramming to Differentiation: A Tale in Cytoplasmic and Nuclear Compartments. Int J Mol Sci. 2019 Apr 24;20(8):2026. doi: 10.3390/ijms20082026. PMID: 31022972; PMCID: PMC6514809

109. Rodrigues CAV, Fernandes TG, Diogo MM, da Silva CL, Cabral JMS. Stem cell cultivation in bioreactors. Biotechnol Adv. 2011;29:815–29

110. Rodríguez-Carballo E, Gámez B, Ventura F. p38 MAPK Signaling in Osteoblast Differentiation. Front Cell Dev Biol. 2016 May 6;4:40. doi: 10.3389/fcell.2016.00040. PMID: 27200351; PMCID: PMC4858538

111. Rohani, L., Borys, B.S., Razian, G. *et al.* Stirred suspension bioreactors maintain naïve pluripotency of human pluripotent stem cells. *Commun Biol* 3, 492 (2020).

112. Romito A, Cobellis G. Pluripotent Stem Cells: Current Understanding and Future Directions. Stem Cells Int. 2016;2016:9451492. doi: 10.1155/2016/9451492. Epub 2015 Dec 20. PMID: 26798367; PMCID: PMC4699068.

113. Romito, A., & Cobellis, G. (2016). Pluripotent Stem Cells: Current Understanding and Future Directions. *Stem cells international*, *2016*, 9451492.

114. Rouse, J., Cohen, P., Trigon, S., Morange, M., Alonso-Llamazares, A., Zamanillo, D., Hunt, T., & Nebreda, A. R. (1994). A novel kinase cascade triggered by stress and heat shock that stimulates MAPKAP kinase-2 and phosphorylation of the small heat shock proteins. *Cell*, *78*(6), 1027–1037.

115. Roux PP, Blenis J. ERK and p38 MAPK-activated protein kinases: a family of protein kinases with diverse biological functions. Microbiol Mol Biol Rev. 2004;68:320–44.

116. Rowles J, Slaughter C, Moomaw C, Hsu J, Cobb MH. Purification of casein kinase I and isolation of cDNAs encoding multiple casein kinase I-like enzymes. Proc Natl Acad Sci U S A. 1991;88:9548–9552. doi: 10.1073/pnas.88.21.9548

117. Rueden CT, Schindelin J, Hiner MC, DeZonia BE, Walter AE, Arena ET, Eliceiri KW. ImageJ2: ImageJ for the next generation of scientific image data. BMC Bioinformatics. 2017 Nov 29;18(1):529. doi: 10.1186/s12859-017-1934-z. PMID: 29187165; PMCID: PMC5708080.

118. Rugg-Gunn, P. J., Cox, B. J., Lanner, F., Sharma, P., Ignatchenko, V., McDonald, A. C., Garner, J., Gramolini, A. O., Rossant, J., & Kislinger, T. (2012). Cell-surface proteomics

identifies lineage-specific markers of embryo-derived stem cells. *Developmental cell*, *22*(4), 887–901.

119. Russ, J.C., Neal, F.B. (2016). The Image Processing Handbook (7th ed.). CRC Press. https://doi.org/10.1201/b18983

120. Rys, J. P., Monteiro, D. A., and Alliston, T. (2016). Mechanobiology of TGFβ signaling in the skeleton. *Matrix Biol.* 5, 413–425. doi: 10.1016/j.matbio.2016.02.002

121. Sakaki-Yumoto M., Liu J., Ramalho-Santos M., Yoshida N., Derynck R. Smad2 Is Essential for Maintenance of the Human and Mouse Primed Pluripotent Stem Cell State. J. Biol. Chem. 2013;288:18546–18560. doi: 10.1074/jbc.M112.446591.

122. Sato, N., Sanjuan, I. M., Heke, M., Uchida, M., Naef, F., & Brivanlou, A. H. (2003). Molecular signature of human embryonic stem cells and its comparison with the mouse. *Developmental biology*, *260*(2), 404–413.

123. Schindelin, J., Arganda-Carreras, I., Frise, E. *et al.* Fiji: an open-source platform for biological-image analysis. *Nat Methods* 9, 676–682 (2012). https://doi.org/10.1038/nmeth.2019

124. Schneider CA, Rasband WS, Eliceiri KW. NIH Image to ImageJ: 25 years of image analysis. Nat Methods. 2012 Jul;9(7):671-5. doi: 10.1038/nmeth.2089. PMID: 22930834; PMCID: PMC5554542.

125. Segalés J, Perdiguero E, Muñoz-Cánoves P. Regulation of Muscle Stem Cell Functions: A Focus on the p38 MAPK Signaling Pathway. Front Cell Dev Biol. 2016 Aug 30;4:91. doi: 10.3389/fcell.2016.00091. PMID: 27626031; PMCID: PMC5003838.

126. Selvaraj S, Mondragon-Gonzalez R, Xu B, Magli A, Kim H, Lainé J, Kiley J, Mckee H, Rinaldi F, Aho J, Tabti N, Shen W, Perlingeiro RC. Screening identifies small molecules that enhance the maturation of human pluripotent stem cell-derived myotubes. Elife. 2019 Nov 11;8:e47970. doi: 10.7554/eLife.47970. PMID: 31710288; PMCID: PMC6845233.

127. Shaw, R. J., Kosmatka, M., Bardeesy, N., Hurley, R. L., Witters, L. A., DePinho, R. A., & Cantley, L. C. (2004). The tumor suppressor LKB1 kinase directly activates AMP-activated kinase and regulates apoptosis in response to energy stress. *Proceedings of the National Academy of Sciences of the United States of America*, *101*(10), 3329–3335.

128. Sheffield J. An Introduction to ImageJ: A Useful Tool for Biological Image Processing and Analysis. *Microscopy and Microanalysis*. 2008;14(S2):898-899. doi:10.1017/S1431927608088752

129. Shen MM. Nodal signaling: developmental roles and regulation. Development. 2007;134:1023–1034. doi: 10.1242/dev.000166.

130. Shengqiang Gao, Bowen Chen, Zhenglin Zhu, Chengcheng Du, Jing Zou, Yaji Yang, Wei Huang, Junyi Liao,PI3K-Akt signaling regulates BMP2-induced osteogenic differentiation of mesenchymal stem cells (MSCs): A transcriptomic landscape analysis, Stem Cell Research,Volume 66, 2023, 103010,

131. Shepherd P, Whithers DJ and Siddle K. Phosphoinositide 3-kinase: the key switch mechanism in insulin signalling. *Biochem J* 333:471-490, 1998. Erratum in Biochem J 335:711, 1998

132. Singh A.M., Reynolds D., Cliff T., Ohtsuka S., Mattheyses A.L., Sun Y., Menendez L., Kulik M., Dalton S. Signaling network crosstalk in human pluripotent cells: A Smad2/3-regulated switch that controls the balance between self-renewal and differentiation. Cell Stem Cell. 2012;10:312–326. doi: 10.1016/j.stem.2012.01.014.

133. Sirenko, O., Cromwell, E. F., Crittenden, C., Wignall, J. A., Wright, F. A., & Rusyn, I. (2013). Assessment of beating parameters in human induced pluripotent stem cells enables quantitative in vitro screening for cardiotoxicity. *Toxicology and applied pharmacology*, *273*(3), 500–507.

134. Sokol SY. Maintaining embryonic stem cell pluripotency with Wnt signaling. Development. 2011 Oct;138(20):4341-50. doi: 10.1242/dev.066209. Epub 2011 Sep 8. PMID: 21903672; PMCID: PMC3177306

135. Srinivasan, A., Toh, Y. C., Loh, X. J., and Toh, W. S. (2016). Substrates and surfaces for control of pluripotent stem cell fate and function. *Adv. Surfaces Stem Cell Res.* 343–380. doi: 10.1002/9781119242642.ch12

136. Stefkova K, Prochazková J, Pacherník J. Alkaline phosphatase in stem cells. Stem Cells Int. 2015;2015:628368. doi: 10.1155/2015/628368. Epub 2015 Feb 12. PMID: 25767512; PMCID: PMC4342173.

137. Štefková K, Procházková J, Pacherník J. Alkaline phosphatase in stem cells. Stem Cells Int. 2015;2015:628368. doi: 10.1155/2015/628368. Epub 2015 Feb 12. PMID: 25767512; PMCID: PMC4342173.

138. Stoddart MJ. Cell viability assays: introduction. Methods Mol Biol. 2011;740:1-6. doi: 10.1007/978-1-61779-108-6_1. PMID: 21468961.

139. Stossi F, Singh PK. Basic Image Analysis and Manipulation in ImageJ/Fiji. Curr Protoc. 2023 Jul;3(7):e849. doi: 10.1002/cpz1.849. PMID: 37498127.

140. Stossi, F., & Singh, P. K. (2023). Basic image analysis and manipulation in ImageJ/Fiji. *Current Protocols*, 3, e849. doi: 10.1002/cpz1.849

141. Tang Y., Jiang Z., Luo Y., Zhao X., Wang L., Norris C., Tian X.C. Differential effects of Akt isoforms on somatic cell reprogramming. J. Cell Sci. 2014;127:3998–4008. doi: 10.1242/jcs.150029

142. Tatapudy, S., Aloisio, F., Barber, D., & Nystul, T. (2017). Cell fate decisions: emerging roles for metabolic signals and cell morphology. *EMBO reports*, *18*(12), 2105–2118.

143. Tesar P. J., Chenoweth J. G., Brook F. A., et al. New cell lines from mouse epiblast share defining features with human embryonic stem cells. Nature. 2007;448(7150):196–199. doi: 10.1038/nature05972.

144. Theunissen, T. W., Powell, B. E., Wang, H., Mitalipova, M., Faddah, D. A., Reddy, J., Fan, Z. P., Maetzel, D., Ganz, K., Shi, L., Lungjangwa, T., Imsoonthornruksa, S., Stelzer, Y., Rangarajan, S., D'Alessio, A., Zhang, J., Gao, Q., Dawlaty, M. M., Young, R. A., Gray, N. S., … Jaenisch, R. (2014). Systematic identification of culture conditions for induction and maintenance of naive human pluripotency. *Cell stem cell*, *15*(4), 471–487.

145. Tsuneyoshi N, Tan EK, Sadasivam A, Poobalan Y, Sumi T, Nakatsuji N, Suemori H, Dunn NR. The SMAD2/3 corepressor SNON maintains pluripotency through selective repression of mesendodermal genes in human ES cells. Genes Dev. 2012 Nov 15;26(22):2471-6. doi: 10.1101/gad.201772.112. PMID: 23154981; PMCID: PMC3505817.

146. Turner N., Grose R. Fibroblast growth factor signalling: From development to cancer. Nat. Rev. Cancer. 2010;10:116–129. doi: 10.1038/nrc2780

147. Uddin S, Ah-Kang J, Ulaszek J, Mahmud D, Wickrema A. Differentiation stage-specific activation of p38 mitogen-activated protein kinase isoforms in primary human erythroid cells. Proc Natl Acad Sci USA. 2004;101:147–52

148. Vallier, L., Alexander, M., & Pedersen, R. A. (2005). Activin/Nodal and FGF pathways cooperate to maintain pluripotency of human embryonic stem cells. *Journal of cell science*, *118*(Pt 19), 4495–4509.

149. Vallier, L., Mendjan, S., Brown, S., Chng, Z., Teo, A., Smithers, L. E., Trotter, M. W., Cho, C. H., Martinez, A., Rugg-Gunn, P., Brons, G., & Pedersen, R. A. (2009). Activin/Nodal signalling maintains pluripotency by controlling Nanog expression. *Development (Cambridge, England)*, *136*(8), 1339–1349.

150. Varzideh F, Gambardella J, Kansakar U, Jankauskas SS, Santulli G. Molecular Mechanisms Underlying Pluripotency and Self-Renewal of Embryonic Stem Cells. Int J Mol Sci. 2023 May 7;24(9):8386. doi: 10.3390/ijms24098386. PMID: 37176093; PMCID: PMC10179698

151. Vitillo, L., Baxter, M., Iskender, B., Whiting, P., & Kimber, S. J. (2016). Integrin-Associated Focal Adhesion Kinase Protects Human Embryonic Stem Cells from Apoptosis, Detachment, and Differentiation. *Stem cell reports*, *7*(2), 167–176.

152. Wang Y, Cheng L, Gerecht S. Efficient and scalable expansion of human pluripotent stem cells under clinically compliant settings: a view in 2013. Ann Biomed Eng. 2014 Jul;42(7):1357-72. doi: 10.1007/s10439-013-0921-4. Epub 2013 Oct 17. PMID: 24132657; PMCID: PMC4436032.

153. Waring MJ, Arrowsmith J, Leach AR, Leeson PD, Mandrell S, Owen RM, Pairaudeau G, Pennie WD, Pickett SD, Wang J, Wallace O, Weir A. An analysis of the attrition of drug candidates from four major pharmaceutical companies. Nat Rev Drug Discov. 2015 Jul;14(7):475-86. doi: 10.1038/nrd4609. Epub 2015 Jun 19. PMID: 26091267.

154. Willert K, Brown JD, Danenberg E, Duncan AW, Weissman IL, Reya T, Yates JR 3rd, Nusse R. Wnt proteins are lipid-modified and can act as stem cell growth factors. Nature. 2003 May 22;423(6938):448-52. doi: 10.1038/nature01611. Epub 2003 Apr 27. PMID: 12717451.

155. Williams AB, Schumacher B. p53 in the DNA-Damage-Repair Process. Cold Spring Harb Perspect Med. 2016 May 2;6(5):a026070. doi: 10.1101/cshperspect.a026070. PMID: 27048304; PMCID: PMC4852800.

156. Wood CD, Thornton TM, Sabio G, Davis RA, Rincon M. Nuclear localization of p38 MAPK in response to DNA damage. Int J Biol Sci. 2009 Jun 16;5(5):428-37. doi: 10.7150/ijbs.5.428. PMID: 19564926; PMCID: PMC2702826.

157. Xu R.-H., Sampsell-Barron T.L., Gu F., Root S., Peck R.M., Pan G., Yu J., Antosiewicz-Bourget J., Tian S., Stewart R., et al. NANOG Is a Direct Target of TGFβ/Activin-Mediated SMAD Signaling in Human ESCs. Cell Stem Cell. 2008;3:196–206. doi: 10.1016/j.stem.2008.07.001

158. Xu, C., Inokuma, M. S., Denham, J., Golds, K., Kundu, P., Gold, J. D., & Carpenter, M. K. (2001). Feeder-free growth of undifferentiated human embryonic stem cells. *Nature biotechnology*, *19*(10), 971–974.

159. Xu, X., Zheng, L., Yuan, Q. *et al.* Transforming growth factor-β in stem cells and tissue homeostasis. *Bone Res* 6, 2 (2018). https://doi.org/10.1038/s41413-017-0005-4

160. Yang J, Jiang W. The Role of SMAD2/3 in Human Embryonic Stem Cells. Front Cell Dev Biol. 2020 Jul 21;8:653. doi: 10.3389/fcell.2020.00653. PMID: 32850796; PMCID: PMC7396709

161. Yaping Sun, Zhiqiang Dong, Taihao Jin, Kean-Hooi Ang, Miller Huang, Kelly M Haston, Jisong Peng, Tao P Zhong, Steven Finkbeiner, William A Weiss, Michelle R Arkin, Lily Y JanSu Guo(2013) Imaging-based chemical screening reveals activity-dependent neural differentiation of pluripotent stem cells
eLife 2:e00508.https://doi.org/10.7554/eLife.00508

162. Yoshida, Y., & Yamanaka, S. (2017). Induced Pluripotent Stem Cells 10 Years Later: For Cardiac Applications. *Circulation research*, *120*(12), 1958–1968.

163. Yu Jin Zhang, A review of recent evaluation methods for image segmentation, *Proceedings of the Sixth International Symposium on Signal Processing and its Applications (Cat.No.01EX467)*, Kuala Lumpur, Malaysia, 2001, pp. 148-151 vol.1, doi: 10.1109/ISSPA.2001.949797.

164. Yu M, Wei Y, Xu K, Liu S, Ma L, Pei Y, Hu Y, Liu Z, Zhang X, Wang B, Mu Y, Li K. EGFR deficiency leads to impaired self-renewal and pluripotency of mouse embryonic stem cells. PeerJ. 2019 Jan 29;7:e6314. doi: 10.7717/peerj.6314. PMID: 30713819; PMCID: PMC6357870.

165. Zarubin T, Han J. Activation and signaling of the p38 MAP kinase pathway. Cell Res. 2005;15:11–8.

166. Zhendong Song, Meijing Wang, Yang Ge, Xue-Ping Chen, Ziyang Xu, Yang Sun, Xiao-Feng Xiong, Tyrosine phosphatase SHP2 inhibitors in tumor-targeted therapies,Acta Pharmaceutica Sinica B,Volume 11, Issue 1,2021,Pages 13-29,

167. Zhu S, Li W, Zhou H, Wei W, Ambasudhan R, Lin T, Kim J, Zhang K, Ding S(2010). Reprogramming of human primary somatic cells by OCT4 and chemical compounds. Cell Stem Cell. 2010 Dec 3;7(6):651-5. doi: 10.1016/j.stem.2010.11.015. PMID: 21112560; PMCID: PMC3812930

168. Zongyong Ai, Baohua Niu, Kui Duan, Chenyang Si, Sile Wang, et al Modulation of Wnt and Activin/Nodal supports efficient derivation, cloning and suspension expansion of human pluripotent stem cells, Biomaterials, Volume 249, 2020, 12001 5

3. Appendix

Representative images for each concentration of each chemical are shown below. Statistical analysis was performed using ANOVA with Prism GraphPad. *P<0.05, n=7-10.

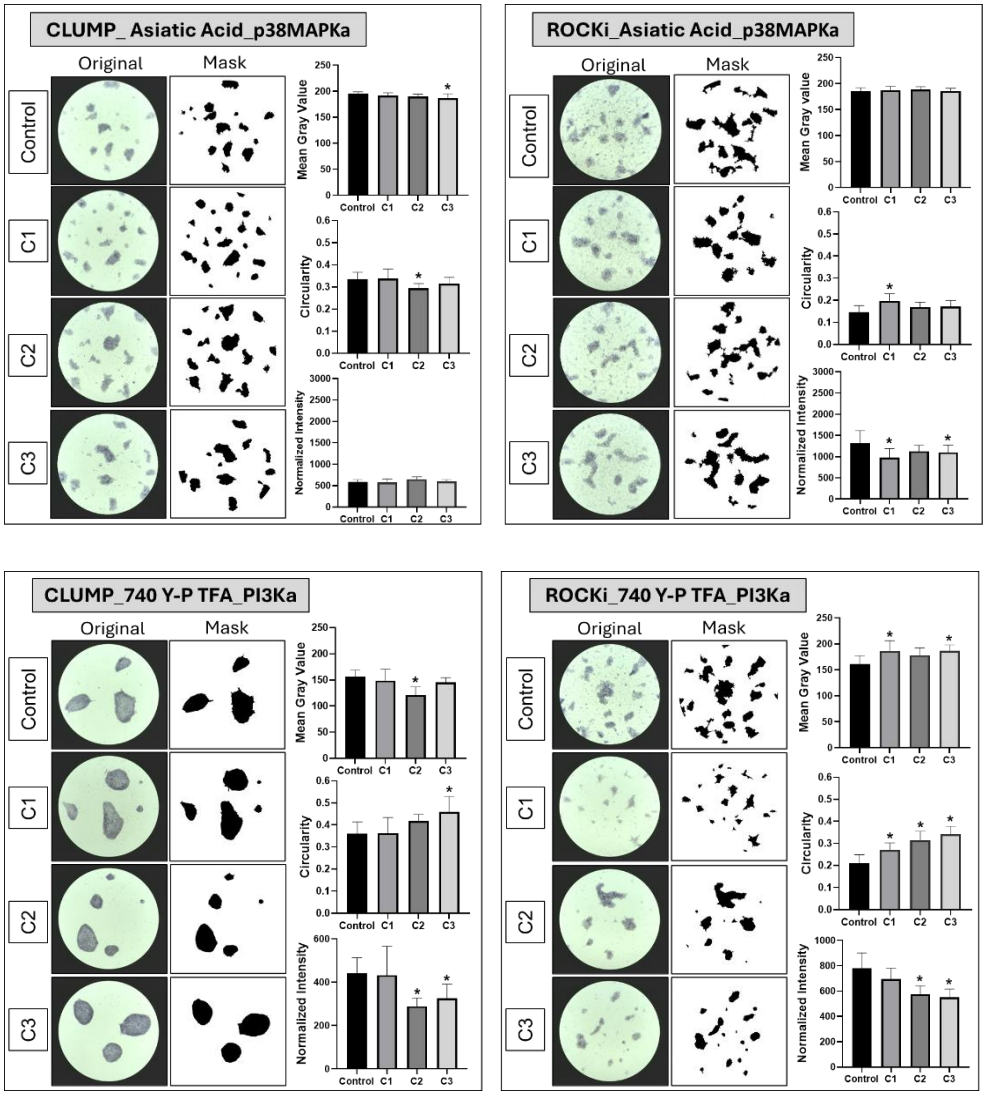

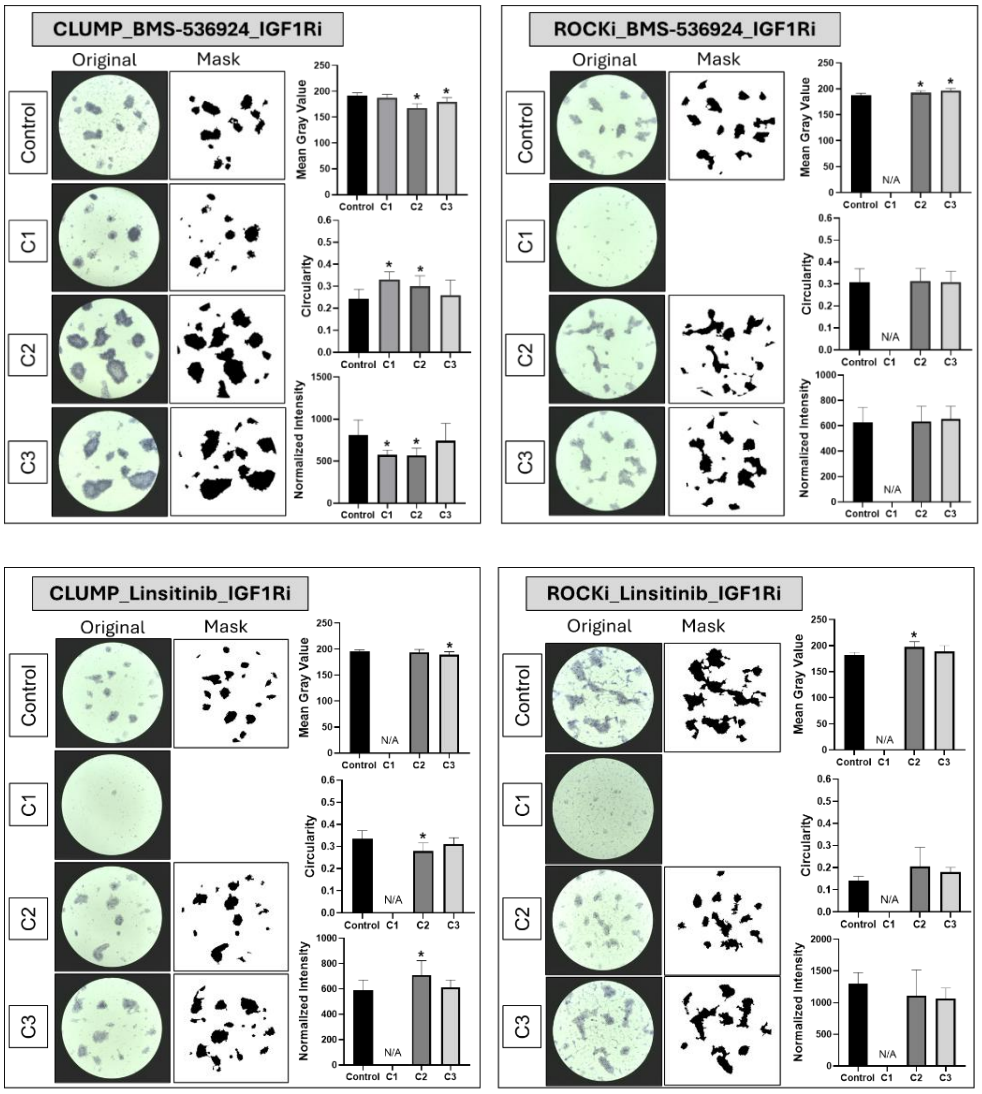
CLUMP_BMS-536924_IGF1Ri
Original
Mask
Control
C1
C2
C3
Mean Gray Value
Circularity
Normalized Intensity
ROCKi_BMS-536924_IGF1Ri
CLUMP_Linsitinib_IGF1Ri
ROCKi_Linsitinib_IGF1Ri
N/A

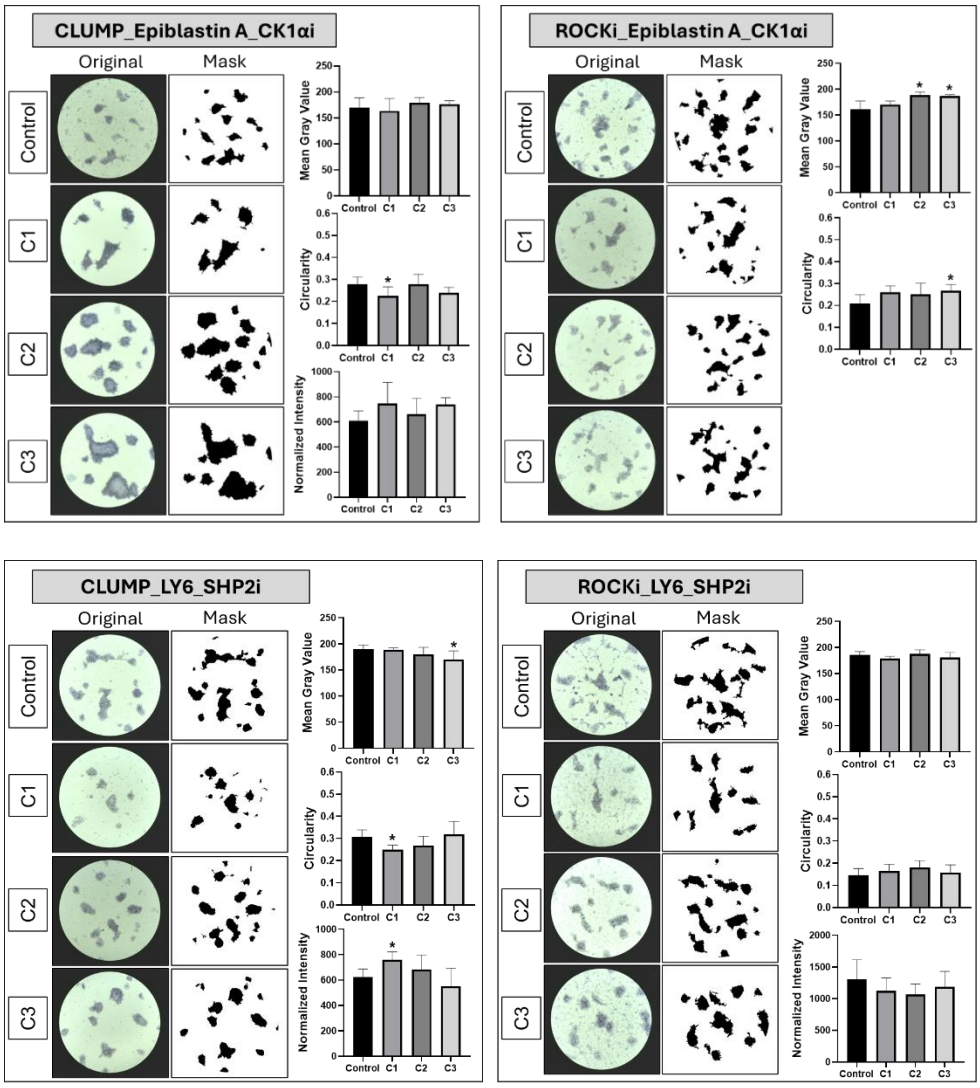
CLUMP_Epiblastin A_CK1αi
Original
Mask
Control
C1
C2
C3
Mean Gray Value
Circularity
Normalized Intensity
ROCKi_Epiblastin A_CK1αi
CLUMP_LY6_SHP2i
ROCKi_LY6_SHP2i

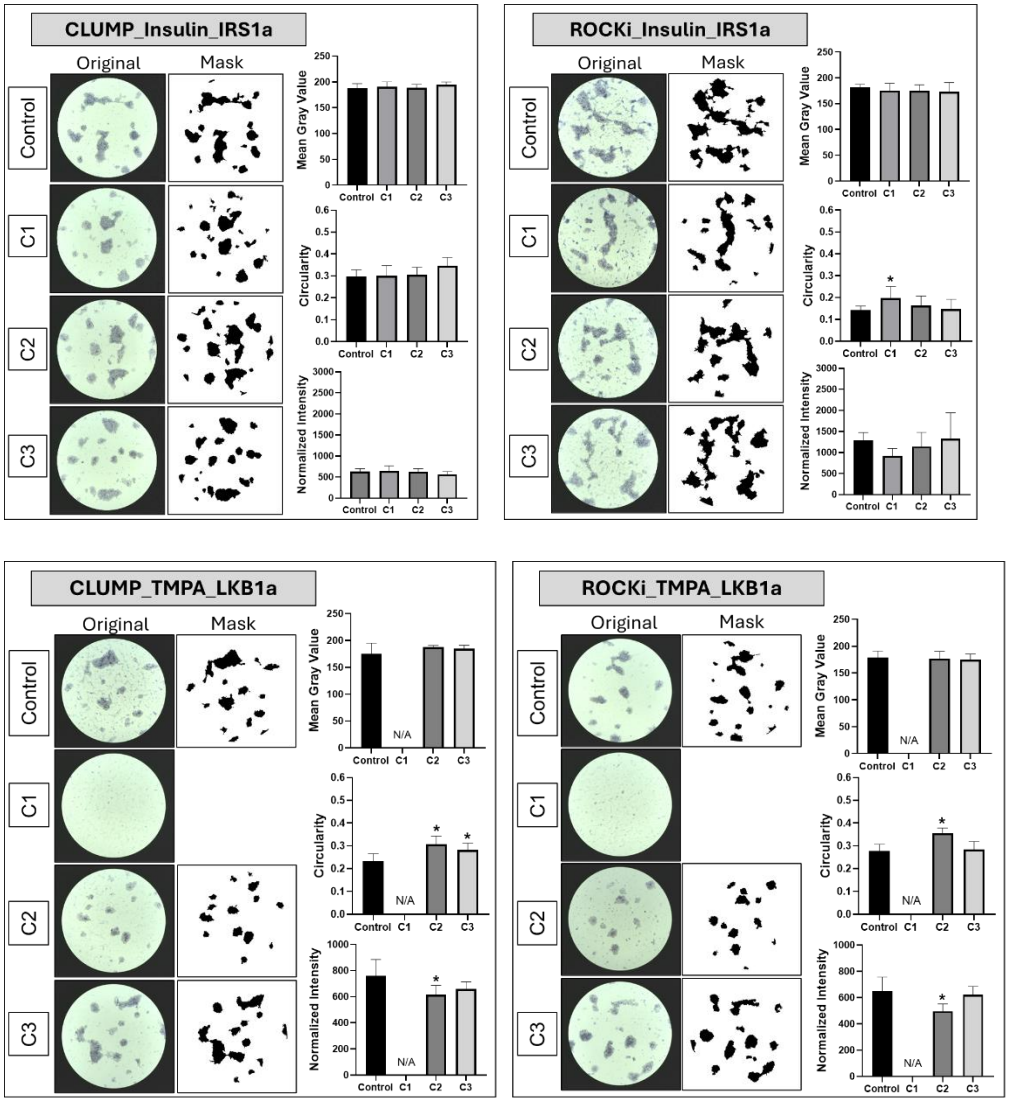
CLUMP_Insulin_IRS1a
Original
Mask
Control
C1
C2
C3
Mean Gray Value
Circularity
Normalized Intensity
ROCKi_Insulin_IRS1a
CLUMP_TMPA_LKB1a
ROCKi_TMPA_LKB1a
N/A

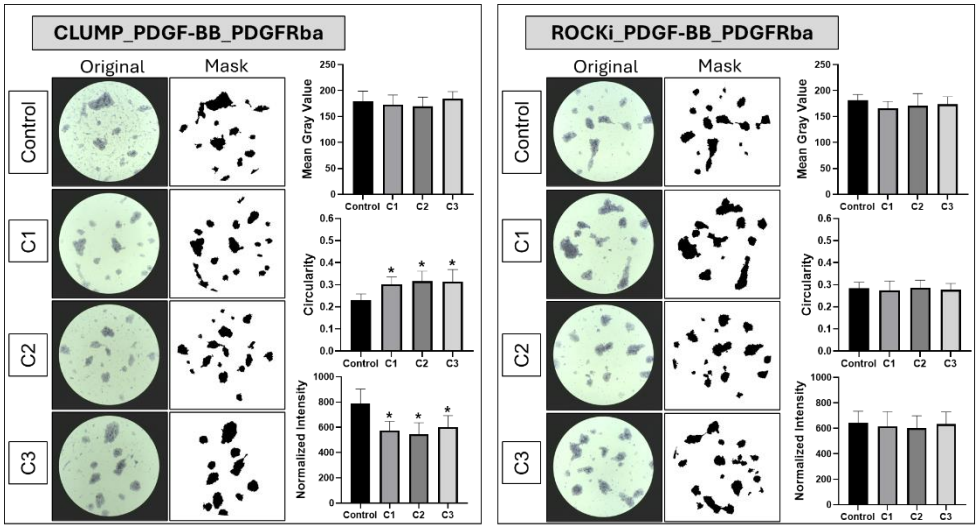
CLUMP_PDGF-BB_PDGFRba
Original
Mask
Control
C1
C2
C3
Mean Gray Value
Circularity
Normalized Intensity
Control C1 C2 C3
ROCKi_PDGF-BB_PDGFRba
Original
Mask
Control
C1
C2
C3
Mean Gray Value
Circularity
Normalized Intensity
Control C1 C2 C3

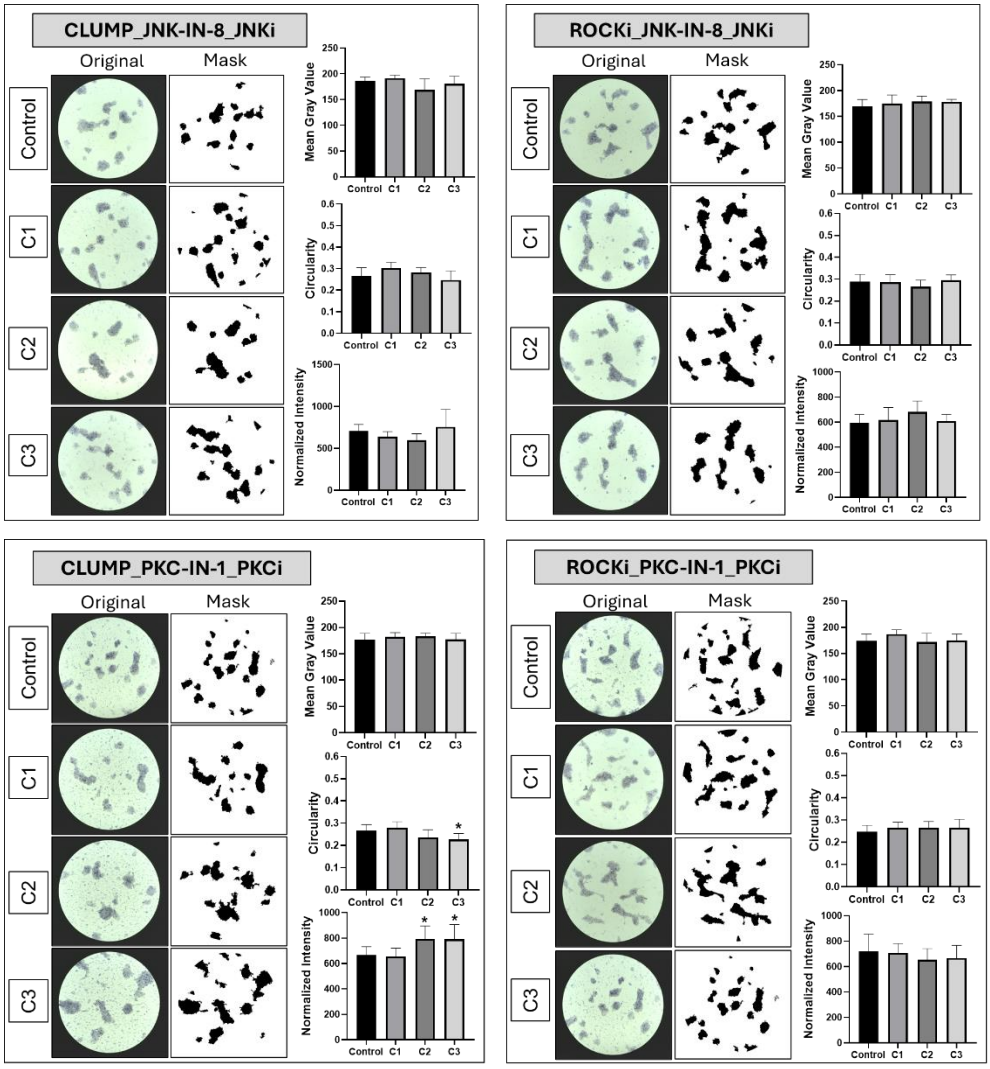
CLUMP_JNK-IN-8_JNKi
ROCKi_JNK-IN-8_JNKi
CLUMP_PKC-IN-1_PKCi
ROCKi_PKC-IN-1_PKCi
Original
Mask
Control
C1
C2
C3
Mean Gray Value
Circularity
Normalized Intensity

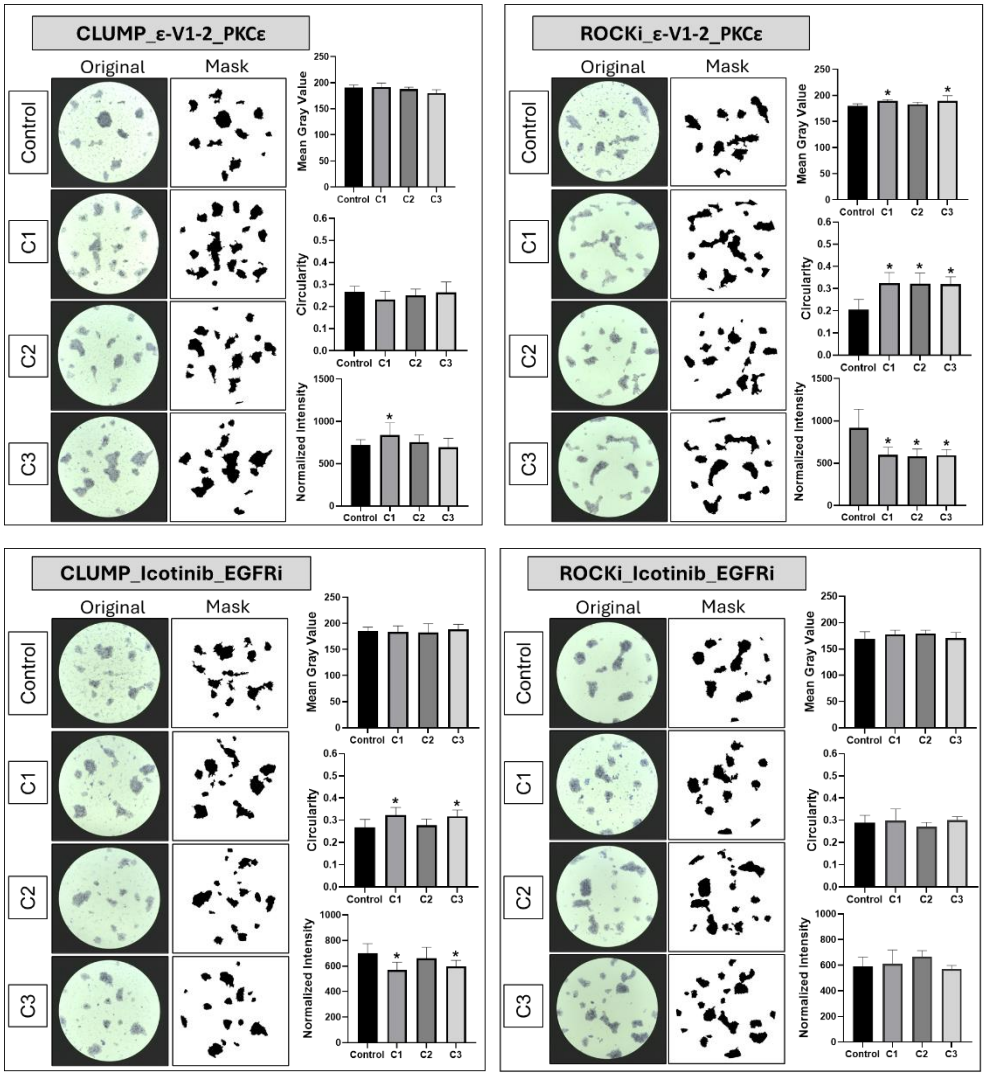
CLUMP_ε-V1-2_PKCε
ROCKi_ε-V1-2_PKCε
CLUMP_Icotinib_EGFRi
ROCKi_Icotinib_EGFRi
Original
Mask
Control
C1
C2
C3
Mean Gray Value
Circularity
Normalized Intensity

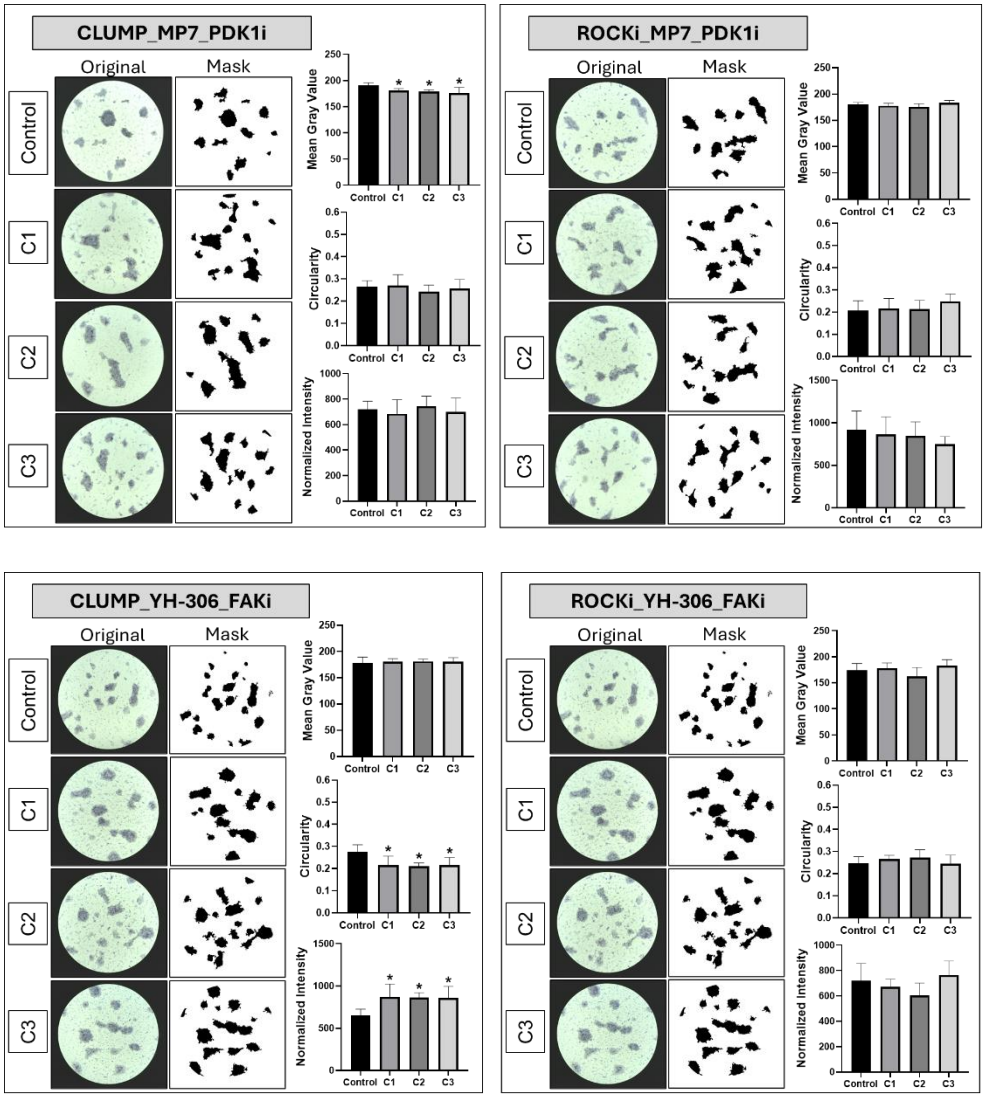
CLUMP_MP7_PDK1i
ROCKi_MP7_PDK1i
CLUMP_YH-306_FAKi
ROCKi_YH-306_FAKi
Original
Mask
Control
C1
C2
C3
Mean Gray Value
Circularity
Normalized Intensity

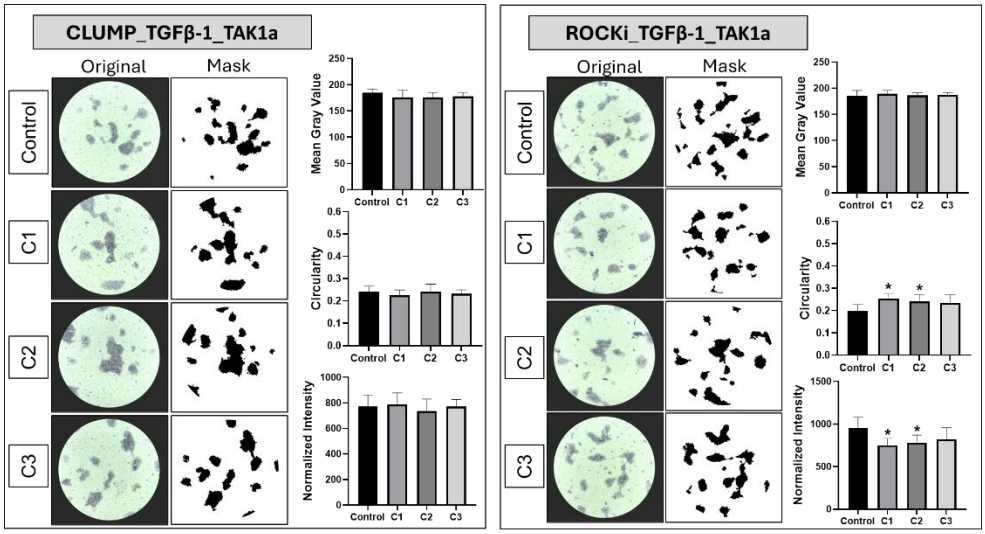
CLUMP_TGFβ-1_TAK1a
Original
Mask
Control
C1
C2
C3
Mean Gray Value
Circularity
Normalized Intensity
ROCKi_TGFβ-1_TAK1a
CLUMP_LY2157299_TGFβi
ROCKi_LY2157299_TGFβi

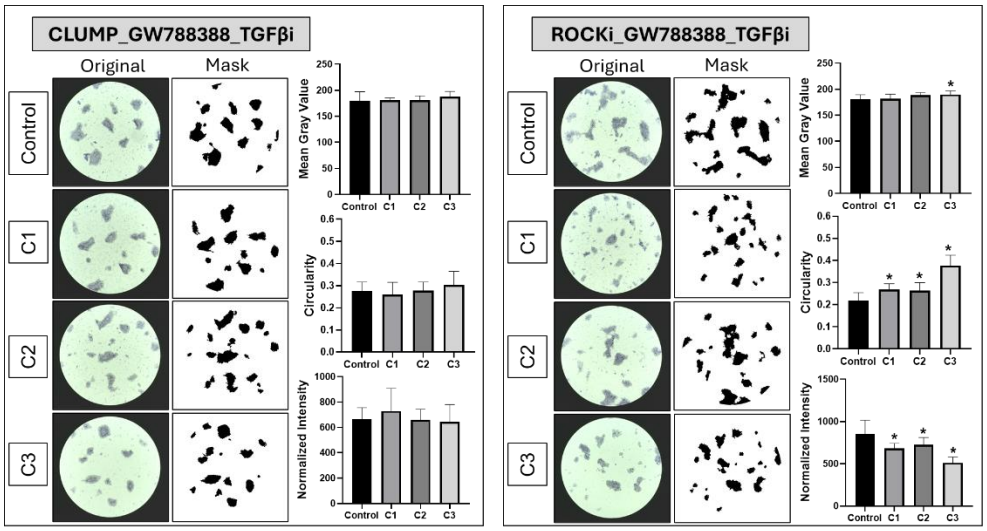
CLUMP_GW788388_TGFβi
Original
Mask
Control
C1
C2
C3
Mean Gray Value
Circularity
Normalized Intensity
Control C1 C2 C3
ROCKi_GW788388_TGFβi
Original
Mask
Control
C1
C2
C3
Mean Gray Value
Circularity
Normalized Intensity
Control C1 C2 C3

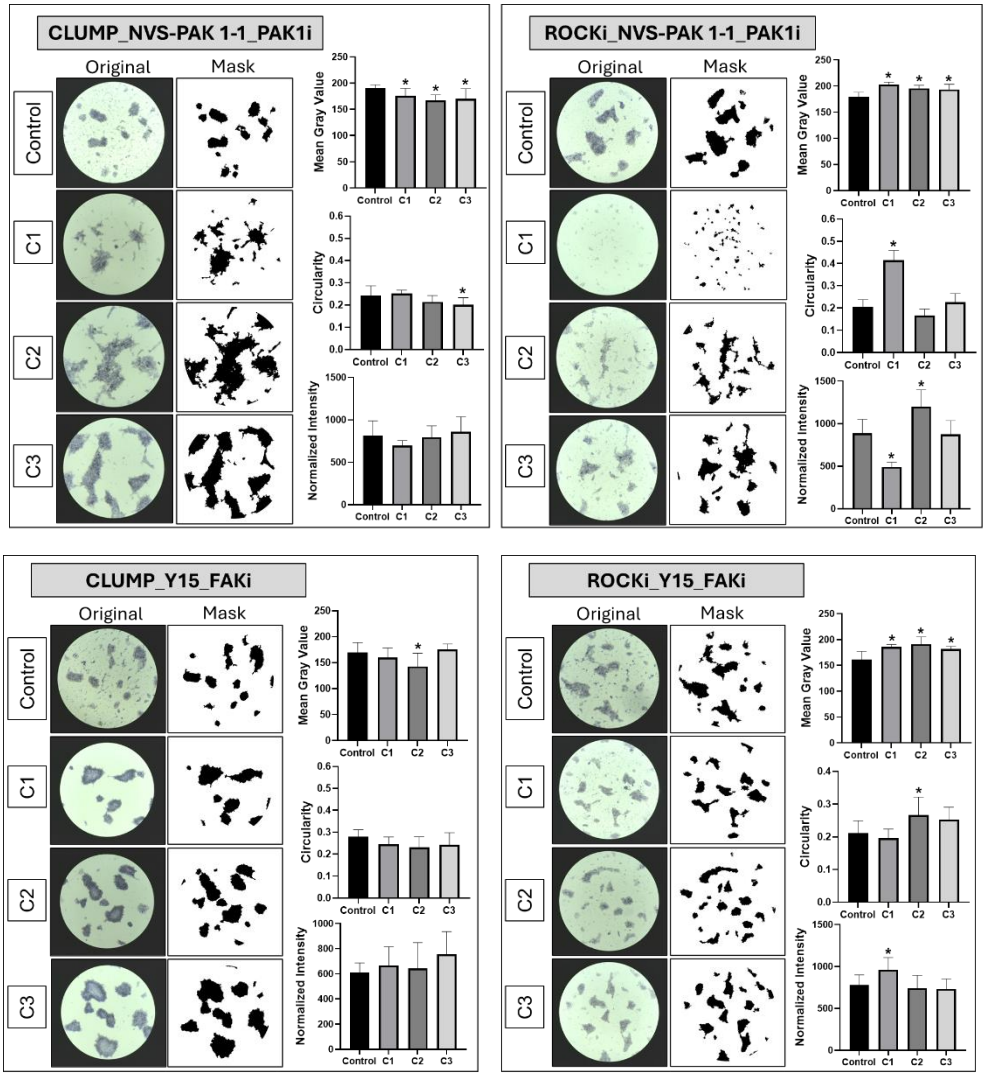
CLUMP_NVS-PAK 1-1_PAK1i
ROCKi_NVS-PAK 1-1_PAK1i
CLUMP_Y15_FAKi
ROCKi_Y15_FAKi
Original
Mask
Control
C1
C2
C3
Mean Gray Value
Circularity
Normalized Intensity

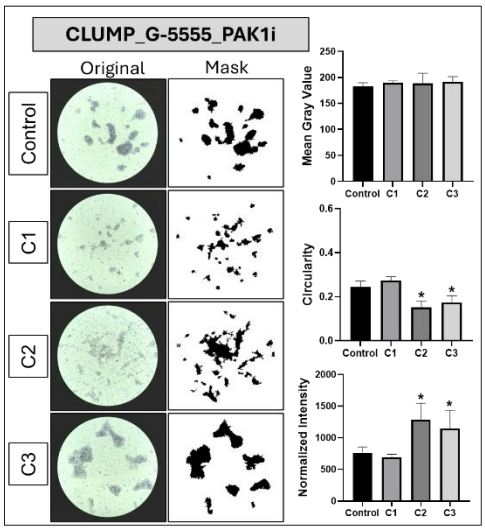
CLUMP_G-5555_PAK1i
Original
Mask
Control
C1
C2
C3
Mean Gray Value
Circularity
Normalized Intensity

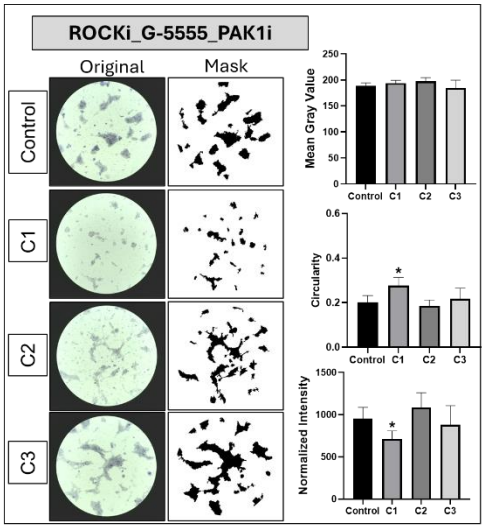
ROCKi_G-5555_PAK1i
Original
Mask
Control
C1
C2
C3
Mean Gray Value
Circularity
Normalized Intensity

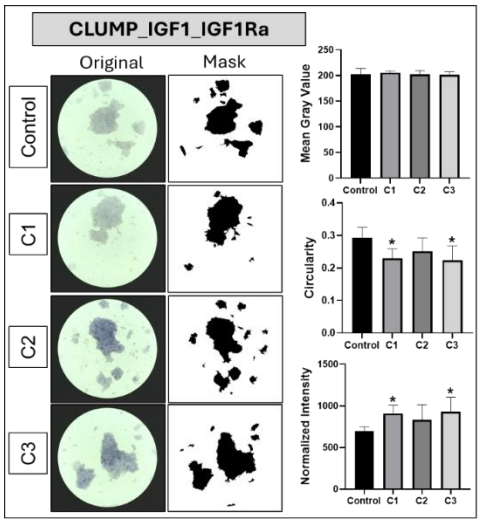
CLUMP_IGF1_IGF1Ra
Original
Mask
Control
C1
C2
C3
Mean Gray Value
Circularity
Normalized Intensity

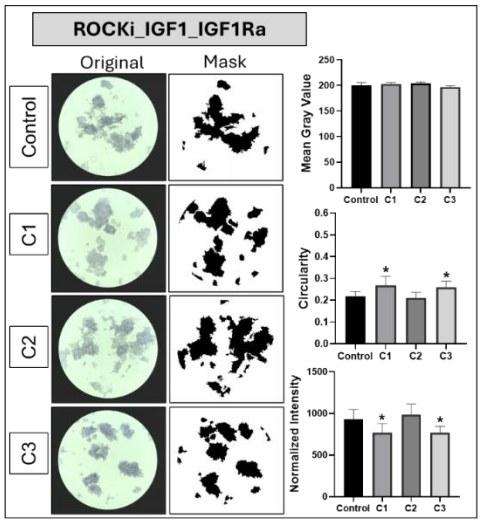
ROCKi_IGF1_IGF1Ra
Original
Mask
Control
C1
C2
C3
Mean Gray Value
Circularity
Normalized Intensity

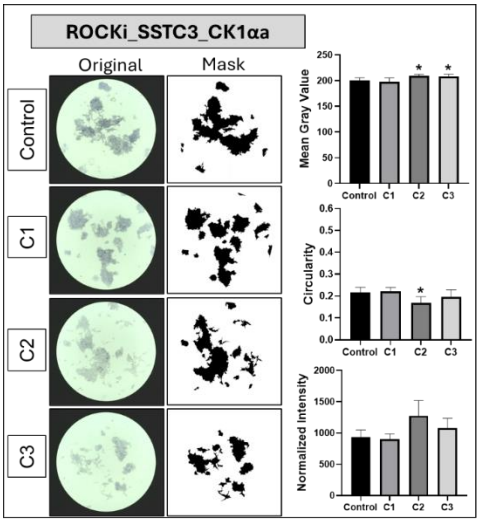
ROCKi_SSTC3_CK1αa
Original
Mask
Control
C1
C2
C3
Mean Gray Value
Circularity
Normalized Intensity

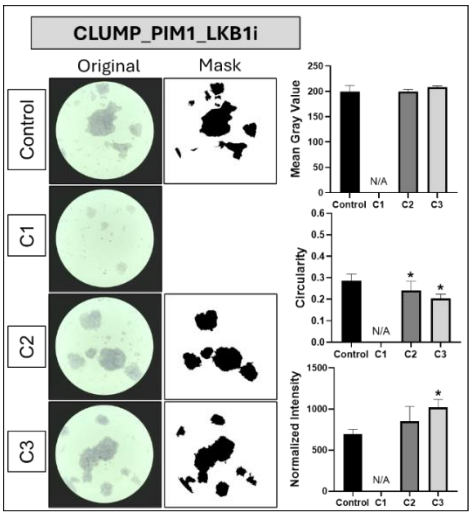
CLUMP_PIM1_LKB1i
Original
Mask
Control
C1
C2
C3
Mean Gray Value
Circularity
Normalized Intensity
N/A
Control C1 C2 C3

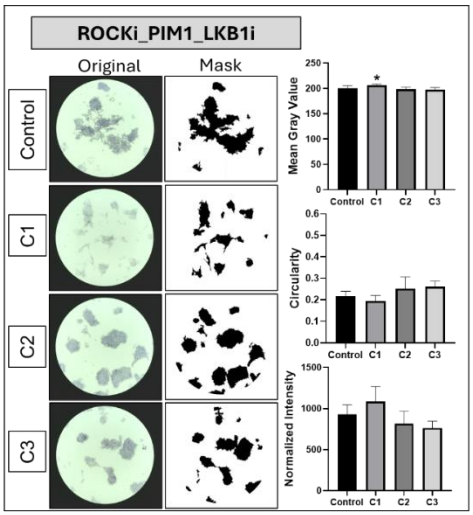
ROCKi_PIM1_LKB1i
Original
Mask
Control
C1
C2
C3
Mean Gray Value
Circularity
Normalized Intensity
Control C1 C2 C3

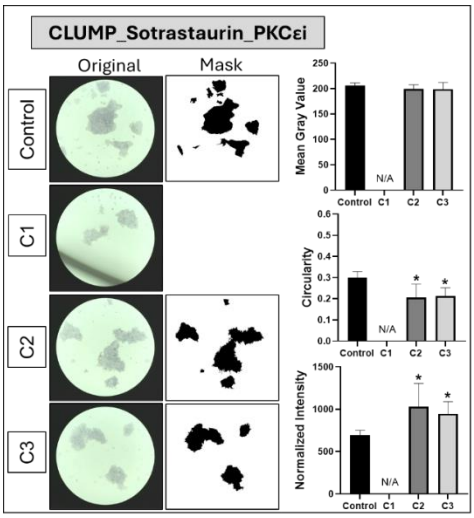
CLUMP_Sotrastaurin_PKCεi
Original
Mask
Control
C1
C2
C3
Mean Gray Value
Circularity
Normalized Intensity
N/A
Control C1 C2 C3

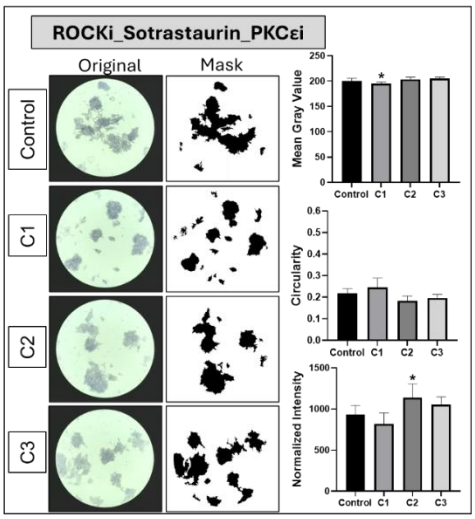
ROCKi_Sotrastaurin_PKCεi
Original
Mask
Control
C1
C2
C3
Mean Gray Value
Circularity
Normalized Intensity
Control C1 C2 C3

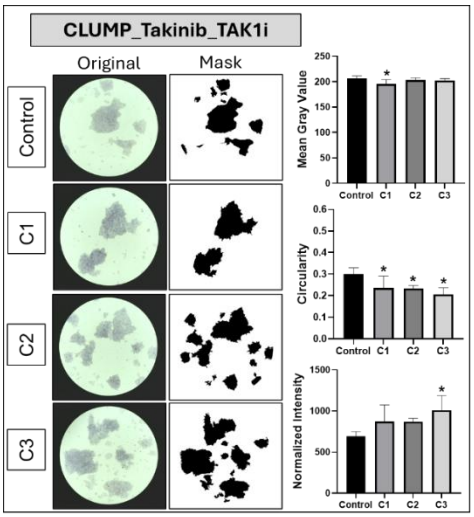
CLUMP_Takinib_TAK1i
Original
Mask
Control
C1
C2
C3
Mean Gray Value
Circularity
Normalized Intensity
Control C1 C2 C3

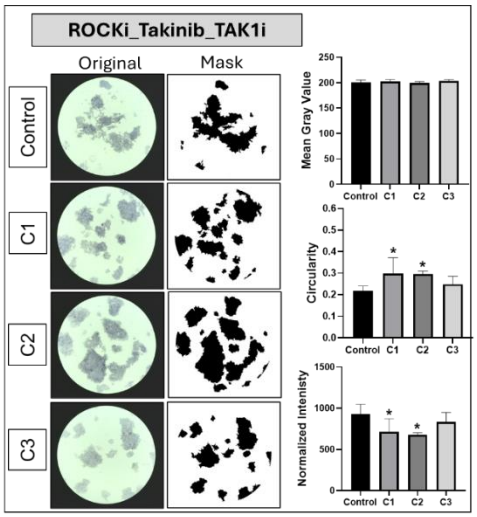
ROCKi_Takinib_TAK1i
Original
Mask
Control
C1
C2
C3
Mean Gray Value
Circularity
Normalized Intensity
Control C1 C2 C3